FINAL REPORT

An Advanced ESTCP PELAN System for Surface and Near-surface UXO Discrimination

ESTCP Project MM-0503

April 2007

Robert Sullivan
Science Applications International Corporation
16701 West Bernardo Drive
San Diego, CA 92127-1309

Approved for public release; distribution unlimited.

Environmental Security Technology Certification Program

An Advanced ESTCP PELAN System for Surface and Near-surface UXO Discrimination

ESTCP Project Number MM-200503

FINAL TECHNICAL REPORT

Revised Version March 2009

Prepared by:
Science Applications International Corporation
10740 Thornmint Road
San Diego, CA 92127

Prepared for:
ESTCP Program Office
901 North Stuart Street, Suite 303
Arlington, VA 22203

VIEWS, OPINIONS, AND/OR FINDINGS CONTAINED IN THIS REPORT ARE THOSE OF THE AUTHOR(S) AND SHOULD NOT BE CONSTRUED AS AN OFFICIAL DEPARTMENT OF THE ARMY POSITION, OR DECISION UNLESS SO DESIGNATED BY OTHER OFFICIAL DOCUMENTATION.

EXECUTIVE SUMMARY

SAIC, in collaboration with Duke University and Environmental Chemical Corporation (ECC), along with Naval Explosive Ordnance Disposal Technology Division, Indian Head (NAVEODTECHDIV) was selected by ESTCP to build, test, demonstrate and validate a mobile, multi-detector-based Pulsed Elemental Analysis with Neutrons (PELAN) unit for the classification of unexploded ordnance (UXO) filler at cleanup sites. Based upon ECC's experience at several cleanup sites to excavate and stockpile UXO for future disposal and disposition, SAIC and ECC recommended to the Environmental Security Technology Certification Program (ESTCP) that the team focus on designing and testing a trailer-mounted system that addressed this immediate need. The development efforts in this redirection would still support future development of a mobile unit for which there is still a need. ESTCP approved this change in direction in December 2005.

The trailer-mounted system design was developed through modeling and testing of various detectors and inspection geometries and shielding. Simulated spectra were modeled for several detector sizes and types, including $LaBr_3$, BGO and NaI. The La-halide crystals have high-energy resolution, fast decay times, and are oxygen free and, therefore, are excellent candidates for the advanced PELAN system. One of the first commercially available 3-inch by 3-inch $LaBr_3$ detectors was purchased from Saint-Gobain Corporation for testing and evaluation in this project. The simulated spectra of the various detectors were analyzed by Duke University using principle component analysis (PCA); divergence metrics were used to compare the separation of features extracted for explosives and inert fills. In general, the prediction showed that BGO detectors had the greatest ability to separate spectral features.

Modeling was also used to determine the signal-to-noise ratio for a variety of setup geometries, neutron/gamma-ray shielding, and moderator material. Emphasis was placed on two approaches: 1) the detection of inelastic gammas from C, O and N in one case and 2) the detection of the 10.8 MeV prompt gamma rays from the nitrogen capture reaction. Based on the results of the modeling, a laboratory test system was designed and assembled at SAIC. Test slugs representing 30mm to 105mm shells were constructed and filled with inert materials and explosives simulants. Both a 3-inch by 3-inch $LaBr_3$ and a 3-inch by 3-inch BGO detector were tested simultaneously. Over 200 measurements were made in the fall of 2006.

Data analysis techniques evaluated in a prior Strategic Environmental Research and Development Program contract were applied to the spectra for feature extraction and to the features for decision making. Both Least Squares analysis (LS) and PCA were applied to the spectra and Generalized Likelihood Ratio Test (GLRT) was used to generate a number of receiver operator characteristic (ROC) curves to evaluate the performance of the $LaBr_3$ and BGO detectors. The results were very good for both detectors, achieving a probability of detection of near 100 percent with probability of false alarm of about 5 percent. Though close in performance, the BGO detector consistently performed better than the $LaBr_3$, mostly due to the higher stopping power of the BGO.

Based upon the results of the experiments, several recommendations were made for designing a trailer-mounted inspection system. System concept drawings were developed and presented at the In-Progress Review on November 1, 2006. Upon review of the results and system design, ESTCP decided to discontinue the effort before the prototype was constructed and demonstrated.

TABLE OF CONTENTS

EXECUTIVE SUMMARY ii
TABLE OF CONTENTS iv
TABLE OF FIGURES v
TABLE OF TABLES v
ACRONYMS vi
ACKNOWLEDGEMENTS i
1. INTRODUCTION 1
1.1 Project Background 1
1.2 Objective 1
1.3 Technical Approach 2
1.3.1 Technical Description 2
1.3.2 The PELAN System 3
2. PROJECT ACCOMPLISHMENTS 4
2.1 System Requirements and Concept 4
2.2 Modeling of System Designs and Detector Responses 7
2.3 Detector Evaluation 10
2.4 Laboratory Test System 19
2.5 Laboratory Testing 19
2.6 Data Analysis 21
2.7 Disposal Cost Examples and Payback Estimates 37
2.8 Final Conceptual Design 38
3. OVERALL CONCLUSIONS 39
4. References 41
5. Points of Contact 42

TABLE OF FIGURES

Figure 1.3-1. The PELAN IV system shown here was used for tests at Indian Head in December 2004. 3
Figure 2.1-1. Original system concept. 4
Figure 2.1-2. Conceptual Transport Methods 5
Figure 2.1-3 Examples of stockpiling conducted at Camp Edwards, Massachusetts Military Reservation (MMR), Cape Cod, MA. 7
Figure 2.3-1. Comparison of energy resolutions of $LaBr_3$, NaI and BGO using a Ba-133 source. 12
Figure 2.3-2. The 3”x3” $LaBr_3$ detector received from Saint Gobain (France). 13
Figure 2.3-3. Comparison of 3”x3” BGO and 3”x3” $LaBr_3$ spectra produced from inelastic neutron reactions in water. 13
Figure 2.3-5. Example fill material feature clusters for the BGO (3×3) detector. 16
Figure 2.3-6. Divergence metric (left) and scatter metric (right) for fill identification. 18
Figure 2.5-1. Test slugs used in the lab testing. 20
Figure 2.5-2. The three detectors used in the lab testing. 21
Figure 2.6-1. Plot of Ratio 2 vs. Ratio 1 from BGO for all slugs with empty in background. 23
Figure 2.6-2. Plot of Ratio 2 vs. Ratio 1 from BGO for all slugs with no empty in background. ..23
Figure 2.6-3. Plots of Ratio 2 vs. 1 for the LS-1 configuration and with no shell in the background. The bottom plot is zoomed in over the blue box in the top plot. 25
Figure 2.6-4. Plots of Ratio 2 vs. 1 for the LS-2 configuration and with no shell in the background. The bottom plot is zoomed in over the blue box in the top plot. 26
Figure 2.6-5. Plots of Ratio 2 vs. 1 for the LS-3 configuration and with an empty shell in the background. The bottom plot is zoomed in over the blue box in the top plot. 27
Figure 2.6-6. Plots of Ratios 2 vs. 1 for the LS-4 configuration and with an empty shell in the background. The bottom plot is zoomed in over the blue box in the top plot. 28
Figure 2.6-7. ROC curves generated using C, H, N, O and Si elemental intensities from the LS results for the BGO and $LaBr_3$ detectors. 30
Figure 2.6-8. ROC curves generated using C/O and H/C elemental intensity ratios from the LS results for the BGO and $LaBr_3$ detectors. 31
Figure 2.6-9. ROC curves generated using elemental intensities and ratios from the LS results for the BGO and LaBr3 detectors. 32
Figure 2.6-10. ROC curves for the PCA and GLRT analysis. 34
Figure 2.6-11. Probability that a fill is correctly identified. 35
Figure 2.6-12. Probability that the fill class is correctly identified. 36
Figure 2.8-1. Software User Interface 39

TABLE OF TABLES

Table 1.3-1. Elemental densities and ratios of three classes of substances. 2
Table 2.2-1. Modeling results of the various configurations. 10
Table 2.3-1. Properties of several scintillators 11
Table 2.3-2. Full energy peak detection efficiencies relative to that of a 3”x3” NaI at 1.33 MeV. 11
Table 2.6-1. LS configurations for analysis of $LaBr_3$ spectra 24

ACRONYMS

ANFO	Ammonium Nitrate - Fuel Oil mixture
AT	Anti-tank
BGO	Bismuth germinate $Bi_3Ge_4O_{12}$
BIP	Blow-in-Place
CDC	Contained Detonation Chamber
COMP B	A mixture of 60% RDX, 39% TNT and 1% wax
CONOPS	Concept of Operations
C-4	Composition C4 (RDX and non-explosive plasticizers)
cps	counts per second
CW	Chemical Warfare agent
d-T	deuterium-tritium
DoD	Department of Defense
DOE	Department of Energy
ECC	Environmental Chemical Corporation
EOD	Explosives Ordnance Disposal
EPA	Environmental Protection Agency
ESTCP	Environmental Security Technology Certification Program
FUDS	Formerly Used Defense Sites
GLRT	Generalized Likelihood Ratio Test
HE	High Explosive
HEAT	High Explosive Anti-Tank
HPGe	High Purity Germanium
IEDs	Improvised Explosive Devices
$LaBr_3$	Lanthanum Bromide Crystal Detector
LS	Least Squares spectral analysis
MCNP	Monte Carlo N-Particle code
MMR	Massachusetts Military Reservation
MMRP	Military Munitions Response Program
MRA	Military Munitions Area
MRS	Military Munitions Site
NaI	Sodium Iodide
NAVEODTECHDIV	Naval Explosive Ordnance Disposal Technology Division, Indian Head
NFI	Non-invasive Filler Identifier (program sponsored by NAVEODTECHDIV)
NG	Neutron generator
PCA	Principal Component Analysis
Pdet or Pd	Probability of Detection
pdfs	Probability Density Functions
PELAN	Pulsed ELemental Analysis with Neutrons
PET	Positron Emission Tomography
Pfa	Probability of False Alarm
PFTNA	Pulsed Fast/Thermal Neutron Analysis
PoP	Plaster of Paris
RDX	Cyclonite (originally known as Royal Dutch Explosives)
ROC	Receiver operator characteristic
ROI	Region of Interest
SAIC	Science Applications International Corporation
SEC	Spider Elemental Counts
SERDP	Strategic Environmental Research and Development Program
SNR	Signal to noise ratio
SPIDER	SPectrum Interpolation and DEconvolution Routine
TERC	Total Environmental Restoration Contract
TGR	Turret Gunnery Range
TNA	Thermal neutron analysis
TNT	Trinitrotoluene

μCi	micro Curies (37,000 decays/second)
UXO	Unexploded Ordnance
WKU	Western Kentucky University

ACKNOWLEDGEMENTS

SAIC would like to acknowledge the contributions of Stacy Tantum and Leslie Collins, of Duke University, in the areas of algorithm development, detector and data analysis. SAIC would also like to thank Doug Lamothe and Glenn Earhart of the Environmental Chemical Corporation for their contributions in the areas of establishing user requirements/concept of operations, providing ordnance specifications and guidance on system design. In addition, SAIC would like to thank Kurt Hacker, Ph.D., for technical oversight and general guidance. SAIC wishes to express its appreciation to ESTCP for funding and supporting this project for UXO discrimination efforts.

1. INTRODUCTION

1.1 Project Background

Prior to the selection of a disposal method for unexploded ordnance (UXO), a determination must be made of the ordnance type (rocket, mortar, projectile, etc.) and whether it is empty or what filler material it contains: practice, inert filler, high explosive (HE), illumination, chemical (i.e., smoke), or chemical warfare agent (CWA). The materials can range from standard military explosives to chemical agents to inert simulants. Currently, trained UXO technicians perform this determination using external markings and visual examination of the construction (i.e., solid base, stake pins, welded base plate). Many times, the UXO has weathered or corroded and the markings and external visual cues are deteriorated or absent. If a positive determination cannot be made that the UXO is free of explosives or chemicals, all questionable UXO is required to be treated as explosive or chemical filled, so the cost of clearance and disposal operations is greatly increased. If a less conservative approach is used, accidents occur, such as those at the Naval Surface Warfare Center, Indian Head Division, and the San Clemente Test Range, that lead to injury or loss of life. There is the need for a means of rapidly and correctly determining the fill of UXO to permit the rapid disposition of inert or empty rounds and proper handling of explosive or chemical-filled UXO.

The Naval Explosive Ordnance Technology Division (NAVEODTECHDIV) has been investigating the use of the Pulsed ELemental Analysis with Neutrons (PELAN) developed by the University of Western Kentucky (WKU) and SAIC as part of an Office of Naval Research Applied Research effort and an Environmental Security Technology Certification Program (ESTCP) effort. These efforts have demonstrated the utility of using PELAN to gather data from explosive-, chemical- and inert-filled UXO, but have highlighted the need for more advanced signal processing to increase the probability of detection and reduce the false alarm rate.

This project addressed Topic 1: Unexploded Ordnance (UXO) Detection, Discrimination, and Remediation in ESTCP's FY05 Broad Agency Announcement released January 8, 2004. The tasks were to design, build, test, demonstrate and validate a mobile, multi-detector-based PELAN unit for the classification of UXO filler at cleanup sites. The goals of these improvements are to increase the filler detection efficiency and accuracy and to reduce false alarm rates, which in turn, would reduce the overall cost of UXO remediation.

1.2 Objective

The overall objective of this project was to design, build, test, demonstrate and validate a mobile, multi-detector-based PELAN unit for the classification of UXO filler at cleanup sites. The following were the main tasks to accomplish this:

- Leverage experience of Environmental Chemical Corporation (ECC) to establish in-field requirements and needs
- Establish conceptual PELAN-based system designs to address need
- Perform Monte Carlo N-Particle (MCNP) modeling to establish optimized design parameters for detector type/size, shielding, moderation and overall configuration

- Construct laboratory experiments to validate modeling efforts
- Work closely with Duke University to evaluate optimal algorithm approach for data analysis
- Construct prototype system, test and demonstrate
- Work closely with NAVEODTECHDIV to establish validation parameters and conduct testing

1.3 Technical Approach

1.3.1 Technical Description

High explosives (TNT, RDX, C-4, etc.) are composed primarily of the chemical elements hydrogen (H), carbon (C), nitrogen (N), and oxygen (O). Many innocuous materials are also primarily composed of these same elements. However, these elements are found in each material with very different elemental ratios and concentrations. It is thus possible to identify and differentiate, for example, TNT from paraffin. Table 1.3-1 shows the atomic density of elements for various materials, along with the atomic ratios. For narcotics, the C/O ratio is at least a factor of two larger than the innocuous materials. Explosives have been shown to be differentiated by utilization of both the C/O ratio and the C/N ratio. The problem of identifying explosives and other threat materials is thus reduced to the problem of elemental identification.

Nuclear techniques present a number of advantages for non-destructive elemental characterization. These advantages include the ability to examine bulk quantities with speed, high elemental specificity, and no memory effects from the previously measured object. These qualities are important for an effective detection system for explosives and drugs.

Neutrons are highly penetrating particles, so their intensity is not diminished significantly by the thickness of commonly utilized containers. Furthermore, the outgoing gamma rays are also very penetrating, easily exiting the interrogated volume. Thus, the method is non-intrusive (the interrogation can take place from a distance of several centimeters) and non-destructive because of the very small amount of radiation absorbed by the interrogated object.

Table 1.3-1. Elemental densities and ratios of three classes of substances.

Density or Ratio	H	C	N	O	Cl	C/O	C/N	Cl/O
Narcotics	High	High	Low	Low	Medium	High, >3	High	Very High
Explosives	Low-Medium	Med	High	Very High	Medium to None	Low, <1	Low, <1	Low to Medium
Plastics	Medium-High	High	High to Low	Medium	Medium to None	Medium	Very High	-

1.3.2 The PELAN System

Developed by WKU with support from NAVEODTECHDIV and other government agencies, PELAN utilizes a pulsing deuterium-tritium (d-T) neutron generator. By using fast neutron reactions, capture reactions, and activation analysis, a large number of elements can be identified in a continuous mode without sampling. PELAN is a man-portable device designed for portability and rapid deployment. Under a program sponsored by a government agency, SAIC extensively upgraded PELAN to improve reliability, ease of use, and data handling. The new, upgraded version, PELAN IV, has been fabricated and has undergone testing in several applications. This system, shown in Figure 1.3-1, consists of two equal-weight portions. The upper section is the neutron generator and accompanying digital control system. The lower section contains the embedded computer, detector system, detector shielding, and operator interfaces such as an Ethernet communication link to a laptop. The controller provides fully automatic operation of PELAN. With a single touch command, all necessary power supplies are energized, neutrons are produced, and data is collected for a predetermined time. Upon the completion of data acquisition, the data are automatically reduced, analyzed, and the results of the interrogation are displayed on the screen.

SAIC has an exclusive license with NuMaT, Inc. and WKU to build and sell PELAN systems. Earlier PELAN prototype systems and the latest PELAN IV have been tested and demonstrated at NAVEODTECHDIV in Indian Head, Md. Over a time span of a couple years, the PELAN was used to acquire over 500 measurements at Indian Head on a variety of shells on a number of different soil types.

Figure 1.3-1. The PELAN IV system shown here was used for tests at Indian Head in December 2004.

2. PROJECT ACCOMPLISHMENTS

2.1 System Requirements and Concept

The original objective of this project was to discriminate between explosive- and inert-filled surface and near-surface UXO. The diagram 2.1-1 illustrates the conceptual PELAN-based approach to address this need.

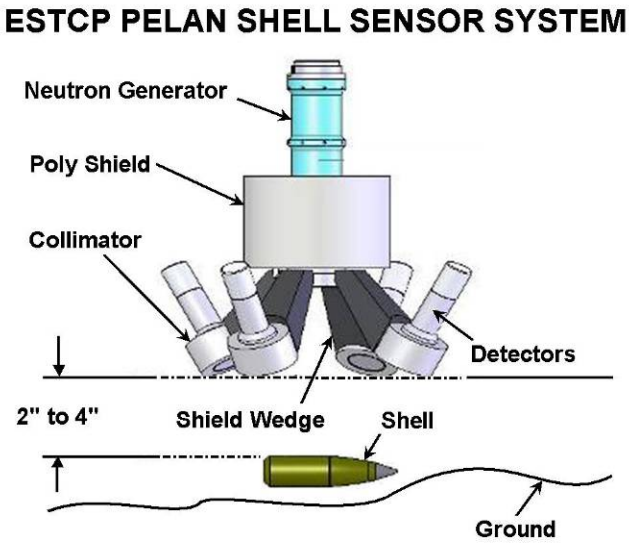

Figure 2.1-1. Original system concept.

The system would be a multi-detector system focused on the ordnance under inspection. Figure 2.1-2 illustrates the various conceptual models proposed for transporting the multi-detector system.

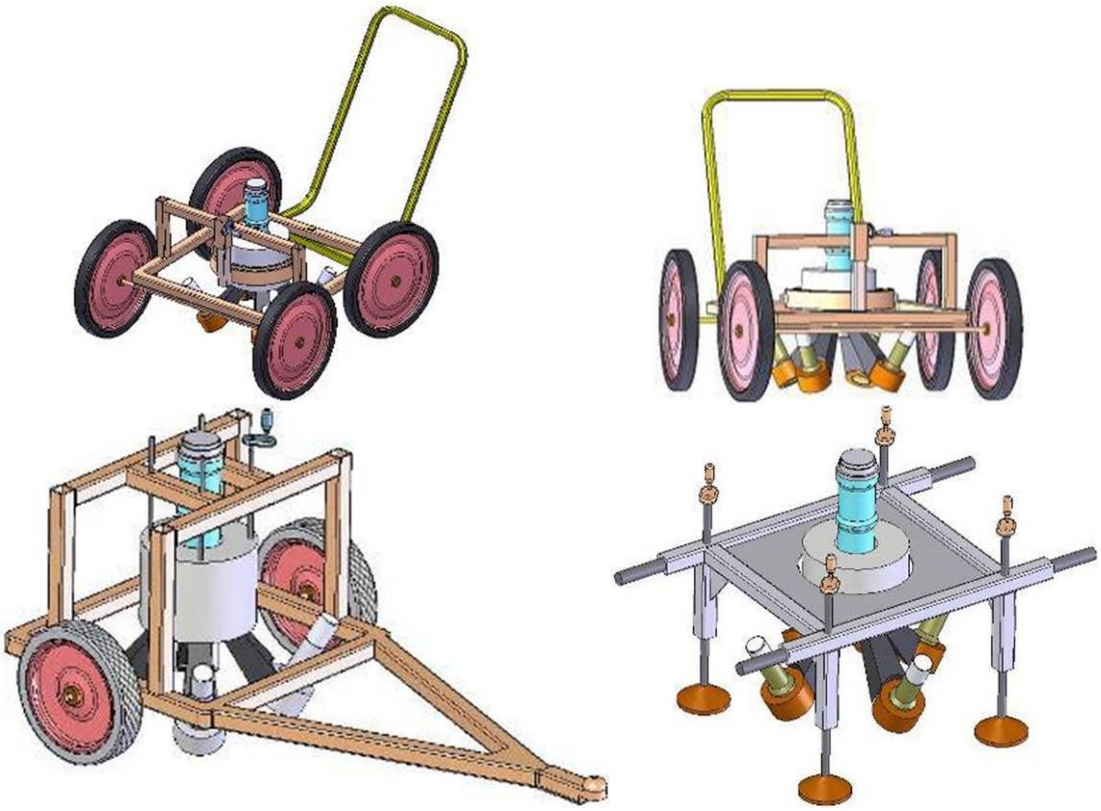

Figure 2.1-2. Conceptual Transport Methods

SAIC teamed with the ECC to leverage ECC's extensive experience in the field of UXO remediation. ECC assisted SAIC in understanding the challenges ECC faced in the field to determine how SAIC's system could aid in saving lives and reducing overall operational costs. ECC identified two basic areas of need:

- Buried UXO (surface, near-surface or sub-surface ordnance that could not be safely excavated, moved or stockpiled which might require blow-in-place (BIP) operations.)

- UXO stockpiled onsite (ordnance that could safely be handled, moved and stockpiled)

UXO/military munitions that are deemed safe to move by qualified military explosive ordnance disposal EOD and/or civilian UXO personnel are sometimes stockpiled at secure locations within military ranges and Military Munitions Response Program (MMRP) project sites to await final inspection and disposition. Stockpiling of recovered UXO, shown in Figure 2.1-3, may occur for various reasons once the items have been inspected and positively identified as acceptable to move and transport within the confines of a military facility or a controlled and secure project site. A few examples of why this action might be taken are

- To remove UXO and munitions debris from active military ranges as expeditiously and safely as possible in order not to negatively impact military training requirements and schedules

- To consolidate quantities of UXO from multiple locations on a specific military munitions site (MRS) to a central consolidation area for future disposal/disposition
- To consolidate quantities of UXO from multiple locations within a military munitions area (MRA) to a central consolidation area for future disposal/disposition

(a) Flags indicate subsurface anomalies along path being cleared for well pad

(b) Example stockpile of mortars pending disposal operations

(c) Another example of projectiles and mortars pending disposal

Figure 2.1-3 Examples of stockpiling conducted at Camp Edwards, Massachusetts Military Reservation (MMR), Cape Cod, Mass.

Based on the current capabilities of the PELAN system and the needs in the field, the team concluded that addressing the onsite stockpiled requirement first would

- Provide a system with a high probability of detection (P_{det} near 100%), thus properly identifying nearly all explosives shells
- Provide a system with a low probability of false alarm (P_{fa} near 5%), thus avoiding the disposal costs associated with identifying an inert munition as an explosive, incendiary, white phosphorous or chemical munition, or a munition with an unknown filler
- Provide valuable information about performance that could later be applied to the buried UXO requirement

2.2 Modeling of System Designs and Detector Responses

Several modeling efforts were conducted using MCNP to address the following major tasks:

- Calculate synthetic spectra of various detectors ($LaBr_3$, BGO and NaI) and sizes to determine, using various analysis techniques, which detector performs the best for this task.
  - The analysis was conducted by Duke University and is described in Section 2.6.
- Model various detector-target-shielding geometries to determine the best setup for filler identification.
  - One model focused on the detection of 10.8 MeV capture gamma ray from nitrogen.
  - The second model focused on detection of inelastic gamma rays from C, N, and O.

Generation of Synthetic Spectra

MCNP modeling was conducted to create synthetic spectra of the various detector spectra for a range of fillers. The geometry was based on one shell size (105mm) in a fixed stationary measurement configuration, with different types of fillers (inert and explosives). The fill type, detector types and sizes, and measurement times were

- Eight filler types
    - Explosives: TNT, RDX, Comp-B
    - Inert: Empty, sand, wax, plaster of Paris (PoP), cement
- Ten detector types and sizes
    - BGO(3x3), BGO(2Lx3D), BGO(5x5)
    - NaI(5x5), NaI(3Lx5D), NaI(3x3)
    - $LaBr_3$ (1.5x1.5), $LaBr_3$ (3x3)
    - HPGe(46.5x45.6), HPGe(60Lx65D)
- Three measuring times
    - One, five, and 10 minutes

A MATLAB® (MathWorks, Inc.) routine was used to extract the output spectra from the MCNP modeling and add noise to the spectra corresponding to a given inspection time. Many spectra for a given fill and detector type could be generated this way for the analysis. The MATLAB routine was provided to the Duke University group so they could generate several hundred spectra for testing the performance differences among the different detectors. The results of the Duke evaluation are discussed in Section 2.3.

Modeling Optimization of 10.8 MeV Capture Gammas from Nitrogen

Because nitrogen is unique to the composition of high explosives found in UXO, the detection of key gamma rays from nitrogen would be a strong discriminator of explosives from inert fills. Because their energy is well above most other gammas produced in neutron reactions and they are highly penetrating, the 10.8 MeV capture gamma rays from nitrogen have been used in several applications for identifying the presence of explosives. Unfortunately, the cross section for this interaction is small (~7 mbarns) for thermal neutrons, so to improve the detection of the 10.8 MeV, the number of detectors and the thermal neutron flux have to be increased. In the current design, we are using two detectors, but it has the flexibility to allow for up to four detectors or more, if needed. To increase the neutron flux with the current neutron generator, we can increase the output of the generator and add a significant amount of moderator material (namely, polyethylene) near and around the UXO. Polyethylene is inexpensive, easy to work with, and contains a large amount of hydrogen, which is most effective at slowing down the 14 MeV neutrons emitted by the neutron generator.

Various modeling configurations were considered. The preferred configurations/geometries have polyethylene added around the target and have the target and detectors positioned closer to the neutron generator.

Experiments were conducted using 3-inch by 3-inch BGO detectors and large 5-inch by 6-inch NaI detectors. For all test slugs (see below for details), no strong N signal was found for short inspection times, so we focused on the detection of inelastic signals from C, N, and O.

Modeling Optimization of Inelastic Gammas from Oxygen, Carbon, and Nitrogen

Each of the potential fill materials contains various amounts of C, H, N, O and Si. Hydrogen has a large capture cross section and is usually easy to identify, and Si in sand or cement/mortar has a strong activation gamma (1.779 keV) that is easy to detect in the thermal spectrum without a large amount of moderator added to the system. C, N and O can be identified through inelastic collisions with the fast neutrons, producing gamma rays that are collected during the neutron pulse. Carbon and oxygen have fairly large (and N fairly small) inelastic reaction cross sections that allow for their detection using the high-energy neutrons emitted by the generator. Because the intensity and ratio of C, O, H and Si can be used to discriminate between the explosives and inert, as demonstrated in testing with UXO at NAVEODTECHDIV, we modeled a set of geometries and shielding materials for optimizing the C, O and N return signals. Twelve separate configurations were modeled for optimizing the signal return from C, N, and O.

Modeling results for the various configurations are summarized in Table 2.2-1. In these results, the detector was a 3-inch by 3-inch BGO detector. The top table shows the number of counts in the 3 to 6.5 MeV region of interest (ROI) where key inelastic gammas from C, O and N are found and for a five-minute measurement. In the bottom table, the signal-to-noise ratios are estimated for each configuration. The column parameters are defined as:

System = gross counts (filler plus background)
Filler = net counts from the filler only
BGO = background counts created by the BGO itself
Bkgrnd = system – filler or the total background

The BGO itself contributes 35% to 53% of the total background caused by reactions of neutrons within the BGO crystal. The largest signal-to-noise ratio (F/sqrt(S)) occurs for configuration number 12. Because the count rate for this configuration is too high for the data acquisition system (resulting in pileup problems), we used Configuration 1 to conduct all of our tests so that pulse pileup effects are reduced.

Table 2.2-1. Modeling results of the various configurations.

Fast Spectra Integration (Using 3x3 BGO) - corrected BGO background

ROI: 3 to 6.5 MeV

Config.No.	System*	Filler	BGO	Bkgrnd	BGO/Bkgrnd
1	2842	1232	559	1610	0.35
2	5083	1508	1710	3574	0.48
3	1348	232	572	1116	0.51
4	2089	483	788	1607	0.49
5	6818	1596	2246	5222	0.43
6	4147	1265	1004	2883	0.35
9	7552	1639	2582	5914	0.44
10	4880	1331	1380	3549	0.39
11	8705	2194	3235	6512	0.50
12	17202	3610	7167	13593	0.53

Relative Fast Spectra Integration

Config.No.	System* (S)	Filler (F)	BGO	Bkgrnd (B)	F/sqrt(S)	F/sqrt(B)
1	1.00	1.00	1.00	1.00	1.00	1.00
2	1.79	1.22	3.06	2.22	0.92	0.82
3	0.47	0.19	1.02	0.69	0.27	0.23
4	0.74	0.39	1.41	1.00	0.46	0.39
5	2.40	1.30	4.02	3.24	0.84	0.72
6	1.46	1.03	1.80	1.79	0.85	0.77
9	2.66	1.33	4.62	3.67	0.82	0.69
10	1.72	1.08	2.47	2.20	0.82	0.73
11	3.06	1.78	5.79	4.04	1.02	0.89
12	6.05	2.93	12.82	8.44	1.19	1.01

With the additional shielding and collimation for the ESTCP setup, the background is reduced by a factor of 10 or more in most regions of the inelastic and thermal spectra, compared to that for the PELAN IV. With this reduction, the signal-to-noise ratio is increased by a factor of 2 to 4. This is a major contribution to the improved sensitivity and performance described in later sections.

2.3 Detector Evaluation

The type and size of gamma-ray detector used in the system affects the performance, based on several characteristic parameters: 1) energy resolution, 2) stopping power (efficiency), and 3) rate of scintillator light decay. The last parameter affects pulse pileup and the count rate limitation and, therefore, the inspection time. That is, if the decay time is fast, the light pulses from the scintillator are less likely to overlap, which helps to maintain the energy resolution to high rates so that data is collected more quickly. The first two characteristics affect the signal-to-noise of the key gamma rays because the narrower the energy resolution, the less noise under the gamma peak and the higher the efficiency, the stronger the signal.

Table 2.3-1 shows properties of some common scintillators (BGO and NaI) and of a new high-speed, high-resolution scintillator, $LaBr_3$. BGO has been used in PELAN because it has

excellent stopping power for high energy gamma rays. However, the energy resolution of BGO is low (it is improving with high-quality crystals and is approaching the energy resolution of NaI). $LaBr_3$ scintillators have excellent energy resolution (about three times that of BGO) and are very fast, but they lack the stopping power for high energy gamma rays.

Table 2.3-2 shows the relative detection efficiencies of various sizes of NaI, BGO, $LaBr_3$ and high-purity Ge (HPGe) detectors. The efficiencies are normalized to that for a 3-inch by 3-inch NaI detector at 1.33 MeV. The HPGe detectors have excellent energy resolution, but they are small in size, require cooling to liquid nitrogen temperatures, and are expensive. The efficiency of detecting a 6 MeV gamma ray is three times greater for a 3-inch by 3-inch BGO crystal than a 3-inch by 3-inch $LaBr_3$ detector. However, because the energy resolution is so much better for $LaBr_3$, we believed $LaBr_3$ was worth evaluating, because the peak and spectral integrity could reveal features that BGO could not.

Table 2.3-1. Properties of several scintillators.

Property	NaI(Tl)	$LaBr_3$ (Ce)	BGO
Density (g/cc)	3.67	5.29	7.13
Zeffective	51	47	74
Light Output (photons/keV)	39	63	9
Resolution @662 keV	6.8%	2.9%	9.5%
Decay time (ns)	230	35	300
Hydroscopic	Yes	Yes	No
Spectral Quality	Med	High	Low
Relative Cost	Low	High	Med
Stopping Power	Med	Med	High
Interferences	Activates	5.1 MeV capture	Oxygen

Table 2.3-2. Full energy peak detection efficiencies relative to that of a 3-inch by 3-inch NaI at 1.33 MeV.

Detector Type (Size)	368 keV	1.33 MeV	6 MeV
$LaBr_3$ (1.5"x1.5")	0.522	0.138	0.026
$LaBr_3$ (3"x3")	2.941	1.362	0.457
HPGe (46.5mmLx45.6mmD)	0.539	0.164	0.033
HPGe (50mmLx50mmD)	0.703	0.226	0.048
HPGe (60mmLx65mmD)	1.400	0.541	0.138
NaI (3"x3")	2.822	1.000	0.259

Detector Type (Size)	368 keV	1.33 MeV	6 MeV
NaI (5"x5")	9.739	4.907	1.951
NaI (3"Lx5"D)	8.151	3.229	1.058
BGO (3"x3")	3.587	2.514	1.363
BGO (2"Lx3"D)	3.340	2.040	0.960
BGO (5"x5")	11.47	9.131	6.214

Initial Evaluation of** 3-inch by 3-inch **$LaBr_3$ Detector

As described above, $LaBr_3$ crystals have two strong advantages over BGO: 1) its energy resolution is three times better and 2) the decay time of the light signal is almost 10 times shorter than for BGO. A comparison among several detector types of the energy resolution is shown in Figure 2.3-1. $LaBr_3$ crystals have been grown in small sizes for a number of years, driven by demands in positron emission tomography (PET), and only until recently, they have become available commercially from Saint-Gobain Corporation in large 3-inch by 3-inch sizes. $LaBr_3$ was developed by Delft University and licensed exclusively to Saint-Gobain for production. When the first crystals became available in April 2006, SAIC requested permission from ESTCP to purchase and test a 3-inch by 3-inch $LaBr_3$ detector. The detector, shown in Figure 2.3-2, arrived in June 2006.

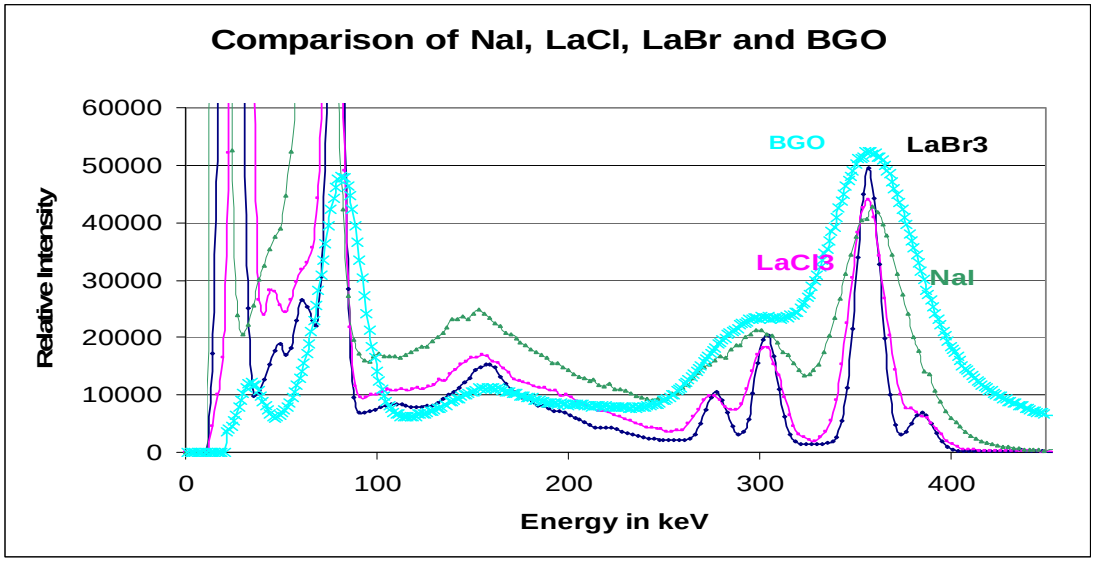

Figure 2.3-1. Comparison of energy resolutions of $LaBr_3$, NaI and BGO, using a Ba-133 source.

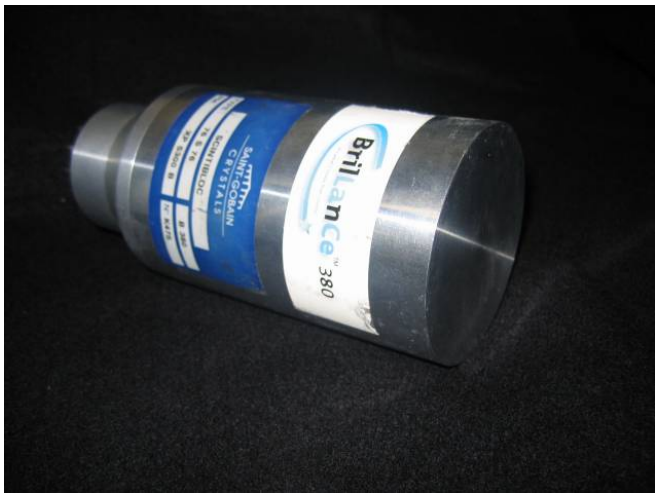

Figure 2.3-2. The 3-inch by 3-inch $LaBr_3$ detector received from Saint-Gobain (France).

The 3-inch by 3-inch $LaBr_3$ detector was evaluated by taking sample spectra of neutron irradiated targets and comparing the spectra with those from a 3-inch by 3-inch BGO. Figure 2.3-3 shows the spectra of the $LaBr_3$ detector and a 3-inch by 3-inch BGO detector for a water target. The energy resolution of the oxygen peak is about 1% for the $LaBr_3$ and 3% for the BGO detector. Across the spectral range, peaks that are not distinguishable in the BGO detector are well separated in the $LaBr_3$ detector.

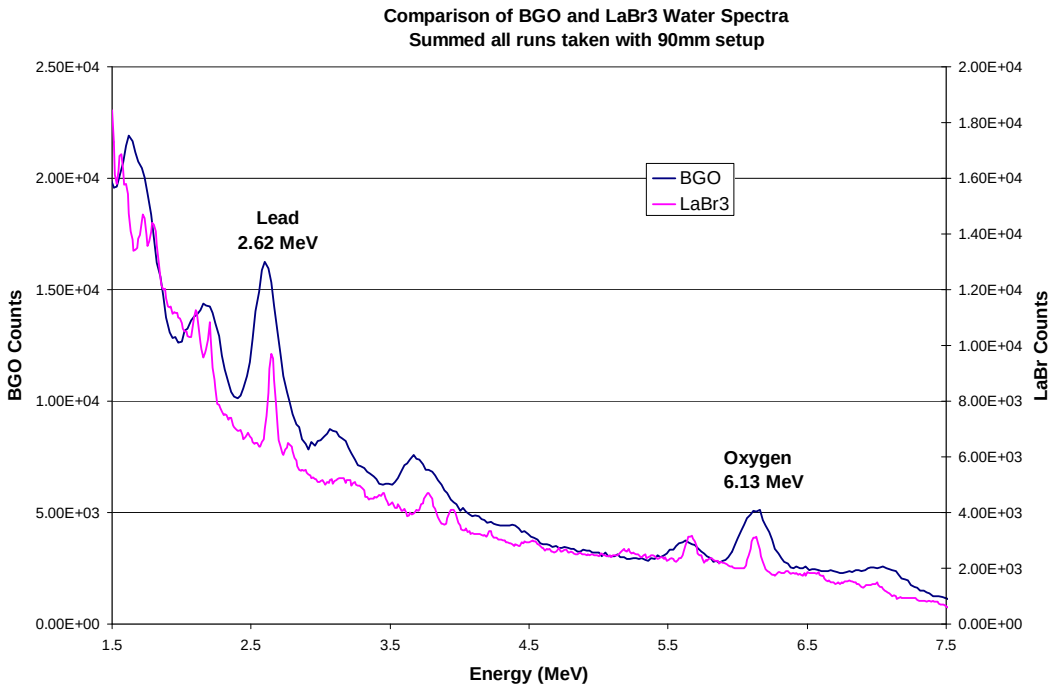

Figure 2.3-3. Comparison of 3-inch by 3-inch BGO and 3-inch by 3-inch $LaBr_3$ spectra produced from inelastic neutron reactions in water.

The 2.313 MeV inelastic line from nitrogen, which is within 100 keV from the 2.2 MeV capture line on hydrogen, was expected to be visible in the $LaBr_3$ spectrum but, because of poorer resolution, would not be separated in the BGO spectrum.

Because these initial test evaluations of $LaBr_3$ showed promise for improved discrimination performance, we continued testing $LaBr_3$ in the lab setups, using simulated explosives and inert-filled slugs.

PCA Analysis Using Simulated Spectra

Using the simulated spectra described in Section 2.2, Duke University applied principal component analysis (PCA) for feature extraction to evaluate the performance obtained by a single detector system. The types and sizes of detectors used were:

- BGO: 3 inches by 3 inches , 2 inches long by 3 inches deep, 5 inches by 5 inches
- $LaBr_3$: 1.5 inches by 1.5 inches, 3 inches by 3 inches
- NaI: 3 inches by 3 inches, 5 inches by 5 inches, 3 inches long by 5 inches deep
- HPGe: 46.5mm by 46.5mm, 60mm long by 65mm deep

The ultimate goal was to choose a set of detectors for a multi-detector configuration that provides robust fill identification performance. The discriminatory capabilities of the multi-detector system are influenced by the capabilities of the component gamma-ray detectors. Thus, this analysis, in which the individual detectors are first analyzed in isolation, was a first step toward that goal. The purpose of this analysis was to identify gamma-ray detectors that provide high discrimination capabilities and to investigate the sources and degree of confusion experienced by each detector. Subsequent analysis will focus on identifying combinations of detectors that generate complementary decisions, or in other words, experience different confusions and, therefore, are good candidates for fusion in a multi-detector system.

The identification capabilities of the detectors were evaluated by investigating the separability of the features describing the fill materials. This approach allowed the relative performance of the individual detectors to be predicted without exhaustive, and time-consuming, simulations to produce confusion matrices and/or receiver operator characteristic (ROC) curves.

The data model utilized to generate simulated data was provided by SAIC. This model for the measured data, m(c), given an underlying signal, As(c), can be expressed as

$$m(c) = \begin{cases} As(c) + \sqrt{As(c)}\eta(c) & As(c) > 50 \\ P(As(c)) & As(c) < 50 \end{cases},$$

where s(c) is the mean detector response for a given fill material, A is a scale factor which is proportional to the time over which data is collected, η(c) is zero-mean Gaussian noise with a standard deviation of 1, and P(As(c)) is Poisson noise with mean As(c). A unique feature of this model is that the measurement noise depends on the underlying signal, As(c). The mean detector response, s(c), is a function of both the detector (size and composition) and the fill material.

This model was employed to generate 500 realizations of the detector response for each detector/fill material combination. The collective data for each candidate gamma-ray detector (all fill materials) was then analyzed using PCA in order to find an efficient representation for the data. Thus, each detector had its own unique set of principal components, and consequently, the full feature set W is unique to each detector.

The ideal feature sets for identification and discrimination are those for which the clusters associated with the target classes do not overlap. In practice, all feature sets will produce target class clusters which overlap to some extent. Thus, the goal was to find a feature set that minimizes the overlap between the target class clusters, or equivalently, maximizes the separability between the clusters. Increased separability leads to improved classification, independent of the specific classification algorithm employed, though the classification performance, itself, is not independent of the specific classification algorithm selected. The ideas of feature separability are best described through an illustrative example. Although the example presented here compares only two different feature sets, and each feature set contains only two elements, the ideas presented here are readily extended to the comparison of multiple M-dimensional feature sets.

For example, the fill material feature clusters for the BGO (3×3) detector are shown in Figure 2.3-5 for the two-element feature sets {W1,W2} and {W1,W3}. These clusters were generated by selecting the desired features ({W1,W2} or {W1,W3}) from the full feature set W and then plotting the features describing the data associated with each fill material in a unique color. From this, it can be seen that the features associated with a given fill material tend to form clusters. Feature set {W1,W2} generally provides larger separability than feature set {W1,W3}. For example, cement is quite distinct from TNT, RDX, and CompB with {W1,W2}, but it is not for {W1,W3}. However, this generalization is not universally true, as illustrated by the clusters for TNT and CompB, which almost completely overlap for {W1,W2}, but are more distinct for {W1,W3}.

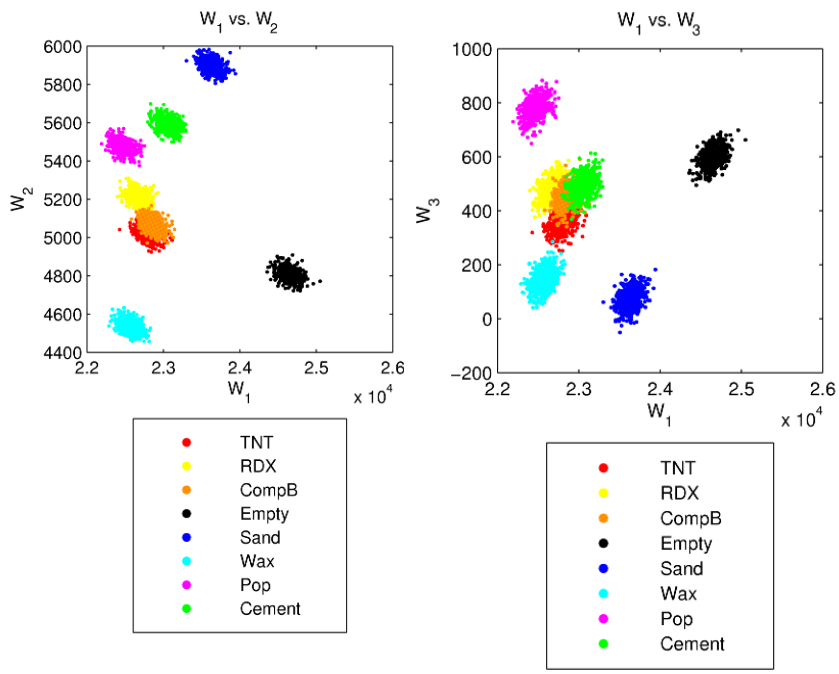

Figure 2.3-5. Example fill material feature clusters for the BGO (3×3) detector.

The separability between two feature clusters was measured quantitatively by evaluating the probabilistic distance between the distributions. Several distance measures have been proposed [1]. The distance measure considered here is the divergence,

$$J_D = \int_{\boldsymbol{x}} [p(\boldsymbol{x}|f_1) - p(\boldsymbol{x}|f_2)] \log\left(\frac{p(\boldsymbol{x}|f_1)}{p(\boldsymbol{x}|f_2)}\right) d\boldsymbol{x},$$

where x represents the feature vector (e.g. {W1,W2}) and f1 and f2 represent the two probability density functions (pdfs) under consideration. For normal distributions described by their means, μ1 and μ2, and covariances, Σ1 and Σ2, the divergence is given by

$$J_D = \frac{1}{2}(\boldsymbol{\mu}_2 - \boldsymbol{\mu}_1)^T(\boldsymbol{\Sigma}_1^{-1} + \boldsymbol{\Sigma}_2^{-1})(\boldsymbol{\mu}_2 - \boldsymbol{\mu}_1) + \mathrm{Tr}\{\boldsymbol{\Sigma}_1^{-1}\boldsymbol{\Sigma}_2 + \boldsymbol{\Sigma}_2^{-1}\boldsymbol{\Sigma}_1 - 2\boldsymbol{I}\}.$$

When the covariances are equal, the divergence reduces to the Mahalanobis distance,

$$J_M = (\boldsymbol{\mu}_2 - \boldsymbol{\mu}_1)^T \boldsymbol{\Sigma}^{-1}(\boldsymbol{\mu}_2 - \boldsymbol{\mu}_1).$$

Low divergence is indicative of closely spaced clusters. The divergence only measures the relative distance between two classes. This example illustrates one of the difficulties in assessing the overall separability of a given feature set; the feature set that maximizes the minimum separability may be different from the feature set that maximizes the mean or median separability. All of these metrics for feature separability measure only the degree of separation

between the classes; they do not provide a measure of the distribution of the pair-wise distances or the spread of the distances for a given feature set.

An alternative approach, which takes into account the spread of the distances, is to use the idea of scatter matrices [1], which are utilized for multiple discriminant analysis [2]. The scatter matrices provide a means to measure the spread of points within each individual feature cluster, termed the within-class scatter (S_W), as well as the spread between the various clusters, the between-class scatter (S_B). A feature set which provides small within-class scatter and large between-class scatter is most desirable. Several metrics based on scatter matrices have been proposed, including the trace of the product of the inverse within-class scatter and the between-class scatter. The definition chosen here is

$$J_{S1} = \mathrm{Tr}\left\{\mathbf{S}_W^{-1}\mathbf{S}_B\right\}$$

The within-class scatter matrix is given by the sum of the within-class scatter matrices for each of the C classes,

$$\mathbf{S}_W = \sum_{c=1}^{C} \mathbf{S}_c,$$

where the within-class scatter matrix for each class is defined by

$$\mathbf{S}_c = \sum_{\mathbf{x}\in c} (\mathbf{x} - \mathbf{m}_c)(\mathbf{x} - \mathbf{m}_c)^T$$

and

$$\mathbf{m}_c = \frac{1}{N_c} \sum_{\mathbf{x}\in c} \mathbf{x}.$$

Three classes of comparisons were considered in the analysis of the simulated spectra:

- Fill material identification
- Explosives versus Inert versus Empty
- Explosives versus Non-explosives filled

Analysis of the simulated data indicated that it is efficiently represented by a small number of principal components. The majority of the variance in the data is explained by the first five principal components. Based on this analysis, only the first 10 principal components were considered candidate features for feature selection. Thus, the feature selection problem is one of choosing K components out of the first 10, where including the higher-order components (components 6-10) does not adversely impact the analysis because they do not contribute significantly to describing the data.

Feature separability was first investigated using divergence as the performance metric. For each value of K, all possible combinations are evaluated and the one combination for which the selected divergence measure is largest is selected. The largest divergence metric (minimum) is plotted as a function of the number of principal components (K) for $1 \leq K \leq 10$ in Figure 2.3-6 on the left.

A similar analysis was performed using scatter matrices as the performance metric. For each value of K, all possible combinations of features are considered and the largest scatter metric for fill identification is plotted as a function of K in Figure 2.3-6 on the right.

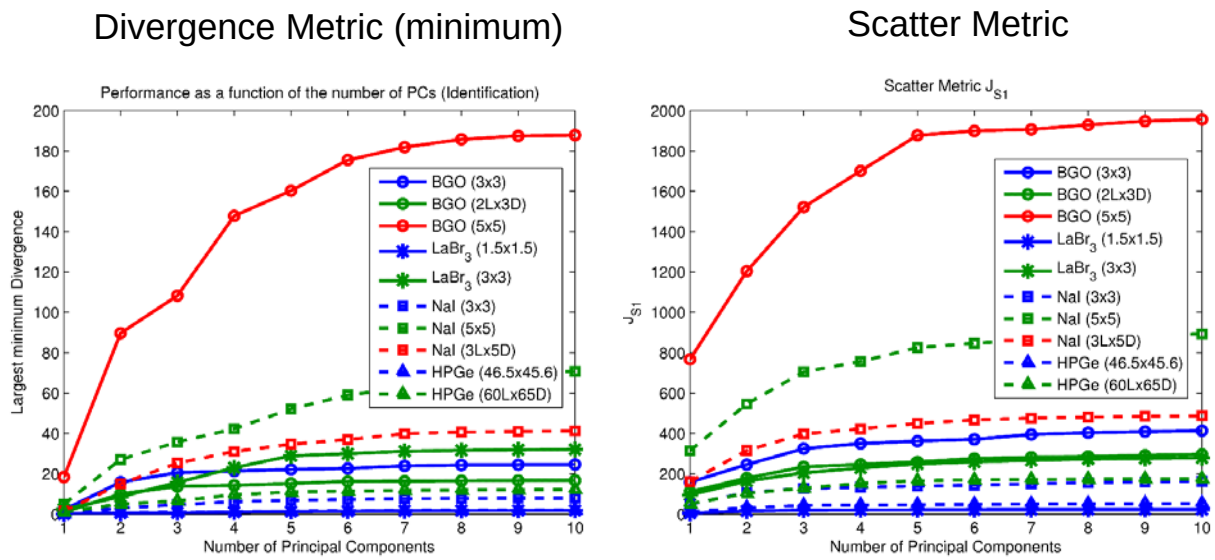

Figure 2.3-6. Divergence metric (left) and scatter metric (right) for fill identification.

The trends seen for the divergence measure are repeated with the scatter measure. As detector size increases, the scatter metric increases, and the detectors follow the same consistent order from largest to smallest separability. In addition, the separability levels off around five to seven components, which is consistent with the previous observation that the data is efficiently represented by the first five principal components.

This analysis focused on determining which gamma-ray detectors provide the best ability to identify fill material when their measured data is analyzed by PCA. For a single detector system, the results suggest that the 3-inch by 3-inch BGO and 3-inch by 3-inch $LaBr_3$ detectors would provide similar performance. In general, detector fusion will successfully improve performance when the component detectors are complementary, meaning they experience different confusions. Recommendations earlier in the program were that future efforts focus on identifying the nature of the confusions experienced by each detector so that fusion of complementary detectors can be explored.

Conclusions for Detector Selection

Based upon the results of the analysis of synthetic spectra and the various sensor geometries, we conclude the following for the experiments with the test slugs.

- For inelastic reactions (C, N, O), use 3-inch by 3-inch $LaBr_3$ and 3-inch by 3-inch BGO.
  - $LaBr_3$ has higher resolution to separate important peaks, but lower stopping power (efficiency).
    - Three-inch by 3-inch $LaBr_3$ was the largest size commercially available.
  - BGO has low resolution, but higher stopping power for high energy gammas (>3 MeV).
  - Larger BGO detectors (e.g., 5"x2") have higher efficiency, but lower energy resolution and cost more.
  - Three-inch by 3-inch BGO detectors were readily available, and we have experience using them (elemental library spectra available for LS).
- For tests to detect 10.8 MeV capture gamma ray from nitrogen, we used 3-inch by 3-inch BGO and 5-inch by 6-inch NaI.
  - Three-inch by 3-inch BGO has good stopping power and smaller volume, so lower background.
  - Five-inch by 6-inch NaI has higher stopping power but larger volume, so higher background.

2.4 Laboratory Test System

Utilizing in-house components and the purchased 3-inch by 3-inch $LaBr_3$ detector, SAIC constructed a laboratory test system. Two experimental setups were evaluated (as were analyzed in MCNP). One configuration focused on inelastic reactions from carbon, oxygen and nitrogen and a separate configuration focused on the 10.8 MeV thermal capture reaction from nitrogen.

A neutron generator, from the portable PELAN unit, was set up at the end of the table and two large shield walls on rolling carts were constructed. The rolling carts allowed for the shield walls to open and close to accommodate various shell sizes. In this configuration, all test slugs constructed (i.e., 30mm to 105mm) were tested. The lead shielding was used to block direct neutron interaction within the gamma-ray detectors. The laboratory system accommodated the 3-inch BGO and $LaBr_3$ detectors as well as the 5-inch NaI detector. The bulk of the data was collected with the 3-inch by 3-inch BGO in Detector Position #1 and the 3-inch by 3-inch $LaBr_3$ in Detector Position #2 for one–to-one detector comparison simultaneously with the same target.

Spectral calibration was maintained by utilizing 0.2 μCi Cs-137 check sources on each detector. Spectral data was collected with either (2) CANBERRA DSA-1000s or (2) APTEC-5000 multi-channel analyzers. The data was post analyzed using both (LS plus General Likelihood Ration Test,GLRT) and (PCA plusGLRT) algorithms as discussed below in Section 2.6: Data Analysis.

2.5 Laboratory Testing

For testing the $LaBr_3$ and BGO detectors and experimental setups for achieving the best performance, SAIC built test slugs which represented the shell size (volume and wall thickness) and fill amount for a range of UXO. The test slugs represented 30mm, 60mm, 81mm, 90mm and 105mm UXO and the volumes of their fill cavities. Information on the fill amount and casing sizes of a range of ordnance shells was provided by ECC and used in the design of the slugs. The

slugs, shown in Figure 2.5-1, were constructed of steel pipes, and steel caps were attached to the ends with epoxy.

The slugs were filled with the following fills:

- Explosives simulants: CompB, TNT
- Inert fillers: wax, mortar, PoP
- Empty

Figure 2.5-1. Test slugs used in the lab testing.

In the testing, two experimental setups were evaluated:

- **Setup 1**
  - Focused on inelastic reactions from C, O, N
  - No moderator material used
  - Three-inch by 3-inch BGO and 3-inch by 3-inch $LaBr_3$ tested simultaneously
- **Setup 2**
  - Focused on 10.8 MeV gamma ray from thermal capture on nitrogen
  - Large amount of polyethylene was added as neutron moderator to increase thermal neutron flux on target
  - Tested 3-inch by 3-inch BGO and 5-inch by 6-inch NaI detectors separately

The three detectors used in the experimental setups are shown in Figure 2.5-2.

In Setup 2, the 3-inch by 3-inch BGO and 5-inch by 6-inch NaI detectors were used because they have reasonable detection efficiencies for the 10.8 MeV capture gamma ray from nitrogen. However, for the range of shells tested here, we found that even with a moderator surrounding the UXO and located behind the neutron generator for increased thermal neutron flux, the 10.8 MeV gamma ray from nitrogen was difficult to detect within the short inspection times. The

reason for the low signal is that the amount of nitrogen in these smaller shells is low and the reaction cross section is small. Therefore, most of the experiments were conducted using Setup 1 for the detection of the inelastic gamma rays from C, N, and O and capture gamma rays from H.

Target measurements were each five minutes long, and the background measurements were 5 minutes or 15 minutes long. Background varies slightly with shell size because the system was adjusted for each size (detectors moved in and out with shell size). Long backgrounds were taken for better peak integrity and statistics in the Least Squares (LS) analysis. Backgrounds were done with no slug present and with an empty slug. Each slug size (except 30mm) and fill was inspected 10 times for over 200 measurements (120 inert, 80 explosives simulants). The signal from the 30mm slugs was too small, so they were not included in the analysis.

Figure 2.5-2. The three detectors used in the lab testing.

2.6 Data Analysis

The analysis of the spectra acquired with the slugs using Setup 1 (inelastic gammas) was conducted in several ways. First, SAIC applied the LS method to the $LaBr_3$ and BGO spectra to extract the elemental intensity features. The elemental intensities and their ratios were plotted to show visually the separation of the explosives simulants and inert features. The original Spectrum Interpolation and Deconvolution Routine (SPIDER) algorithm developed by WKU was used for analysis of the BGO spectra, but it could not be applied to the $LaBr_3$ data because SPIDER was limited to analyzing spectra of 512 channels or less. Because of their higher energy resolution, the $LaBr_3$ spectra were collected with 1,024 channels compared to 512 for the

BGO detector. The LS method and energy calibration scheme had to be developed for the $LaBr_3$ spectra. This was conducted with internal funds from SAIC's internal R&D program.

In the second approach, SAIC provided all of the LS results and spectral data for the BGO and $LaBr_3$ detectors to Duke University so that they could apply GLRT to the LS results and PCA to the spectra. From the GLRT analysis of various combinations of the LS and PCA features, Duke produced several ROC curves to show the performance capability.

BGO LS Results

In the LS analysis of BGO, the standard analysis was performed on the fast (or inelastic) and thermal capture spectra. These parameters, used with or without an empty in the background, are summarized below.

- Group 1: Fast spectrum
    - ROI: 2.4 to 11 MeV
    - Elements: C, N, O, H
- Group 2: Thermal spectrum
    - ROI: 1.1 to 3.5 MeV
    - Elements: H, Si, Ca

The H from Group 2 was used in the analysis. Plots of the elemental intensity ratios from the LS results for the BGO detector are shown in Figures 2.6-1 and 2.6-2, with an empty slug used in the background and with no shell in the background, respectively. All slug sizes are included in these plots. In both plots, the explosives simulants, shown with a box drawn around their values, are clearly separated from the inert. In Figure 2.6-2, the explosives simulants are spread out more, and some results of the empties (60mm or 81mm slugs) fall within the box. In the final system, the empty shells can be sorted by comparing their elemental intensity values against a minimum threshold value. The results indicate that the system is separating the inert and explosives simulants very well.

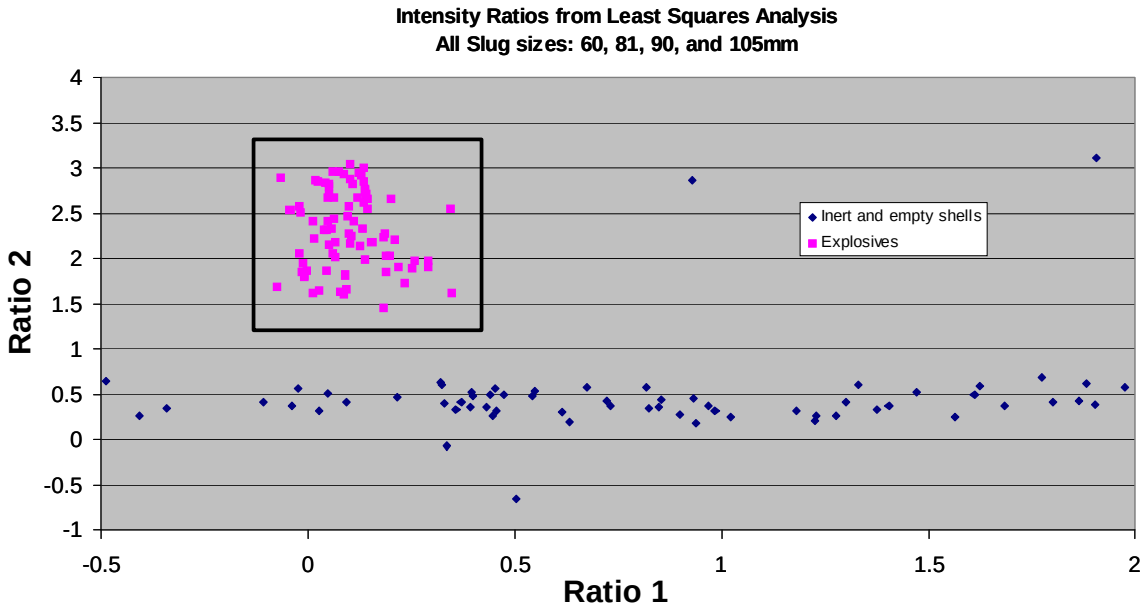

Figure 2.6-1. Plot of Ratio 2 versus Ratio 1 from BGO for all slugs with empty in background.

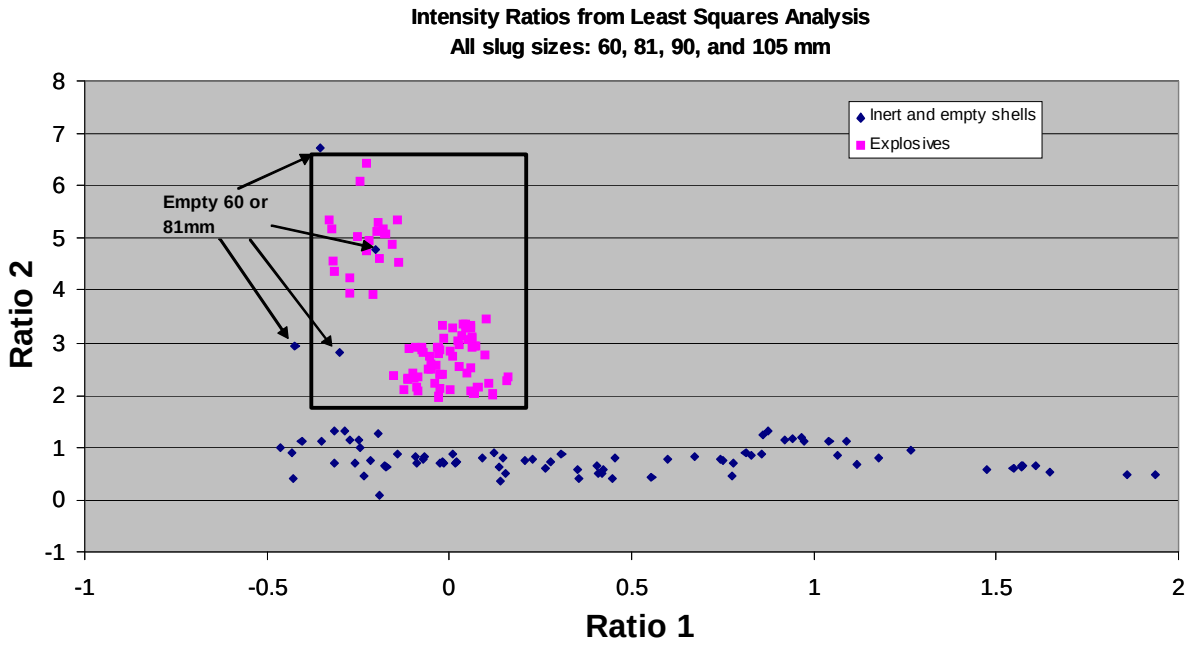

Figure 2.6-2. Plot of Ratio 2 versus Ratio 1 from BGO for all slugs with no empty in background.

$LaBr_3$ LS Results

The LS method for the $LaBr_3$ spectra was developed with SAIC funds. In addition, the method to adjust the energy calibration to a standard for all spectra before running through the LS also

had to be developed. Using select targets, SAIC also developed elemental library spectra for C, N, O, Fe, Al, and Si for use in the LS analysis.

Several different configurations of the LS analysis were evaluated for $LaBr_3$, with and without an empty in the analysis. In these configurations, the ROI for the fast (inelastic) and thermal capture spectra were defined differently. Four of the most promising configurations are shown in Table 2.6-1 below. The various configurations evaluated, for example, the effect of the ROI width on the elemental intensities and how they and their ratios separate explosives from inert.

Table 2.6-1. LS configurations for analysis of $LaBr_3$ spectra.

	Group 1			Group 2			Group 3		
Name	**Spect Type**	**ROI (MeV)**	**Elements**	**Spect Type**	**ROI (MeV)**	**Elem**	**Spect Type**	**ROI (MeV)**	**Elem**
LS-1	Fast	1-8	C,N,O,Fe,Al,Si	Thermal	1.8-3	H	None		
LS-2	Fast	1-8	C,N,O,Fe,Al,Si,Si-act,H	Thermal	1.9-3	H	None		
LS-3	Fast	3-8	C,N,O,Fe,Al,Si	Thermal	1.9-3	H	None		
LS-4	Fast	3-8	C,N,O,Fe,Al,Si	Thermal	1.9-3	H	Fast	3.8-5	C,Fe

Plots of two elemental ratios are shown in Figures 2.6-3 to 2.6-6 for configurations LS-1, LS-2, LS-3, and LS-4, respectively. No shell is used as a background in Figures 2.6-3 and 2.6-4, and an empty shell is used in Figures 2.6-5 and 2.6-6.

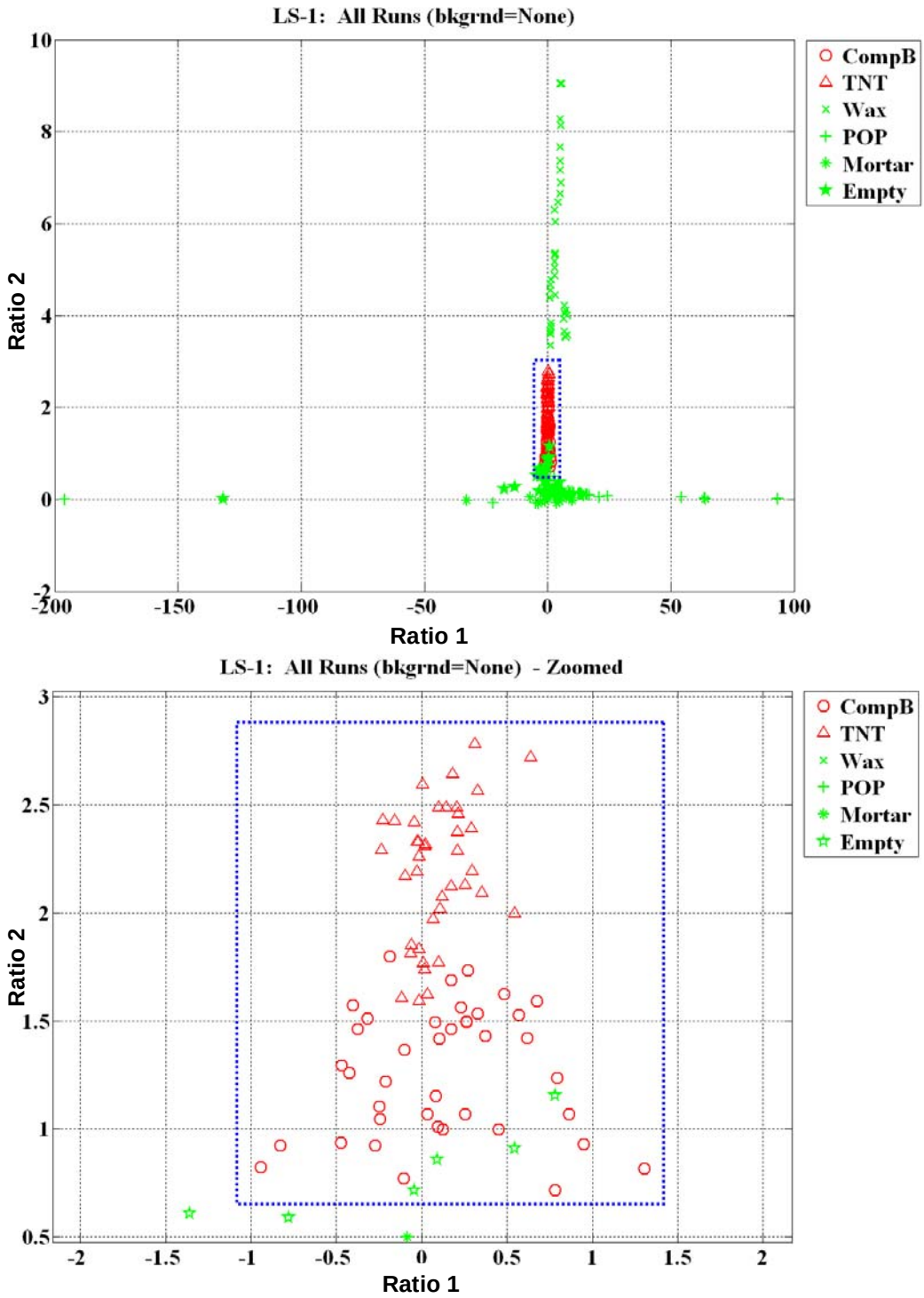

Figure 2.6-3. Plots of Ratio 2 versus 1 for the LS-1 configuration and with no shell in the background. The bottom plot is zoomed in over the blue box in the top plot.

a

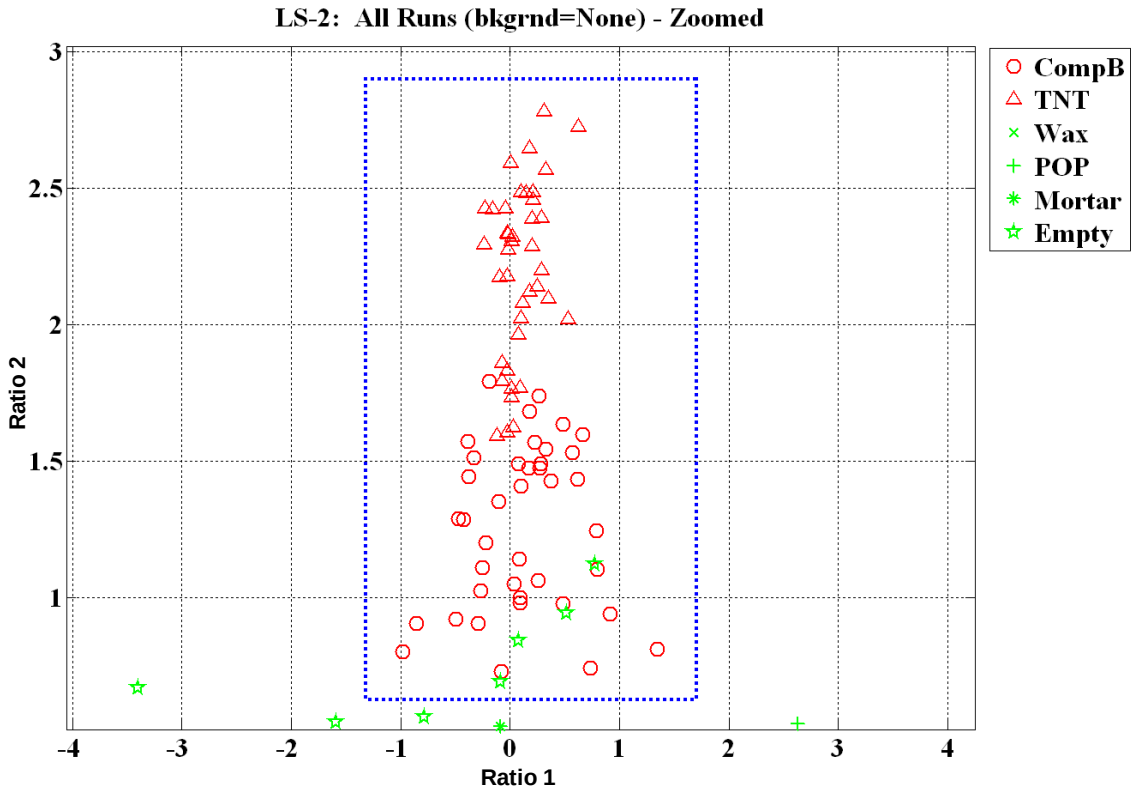

Figure 2.6-4. Plots of Ratio 2 versus 1 for the LS-2 configuration and with no shell in the background. The bottom plot is zoomed in over the blue box in the top plot.

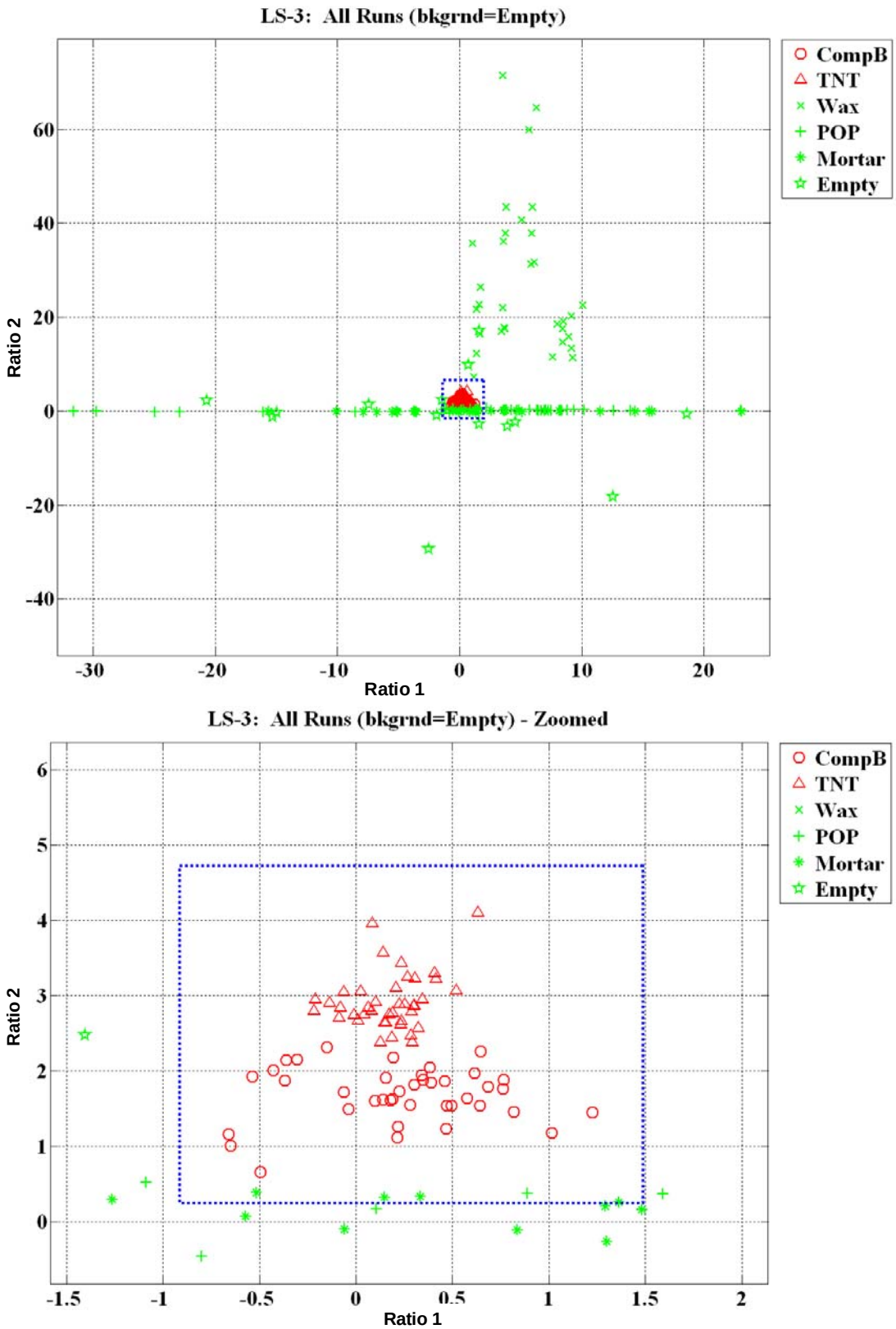

Figure 2.6-5. Plots of Ratio 2 versus 1 for the LS-3 configuration and with an empty shell in the background. The bottom plot is zoomed in over the blue box in the top plot.

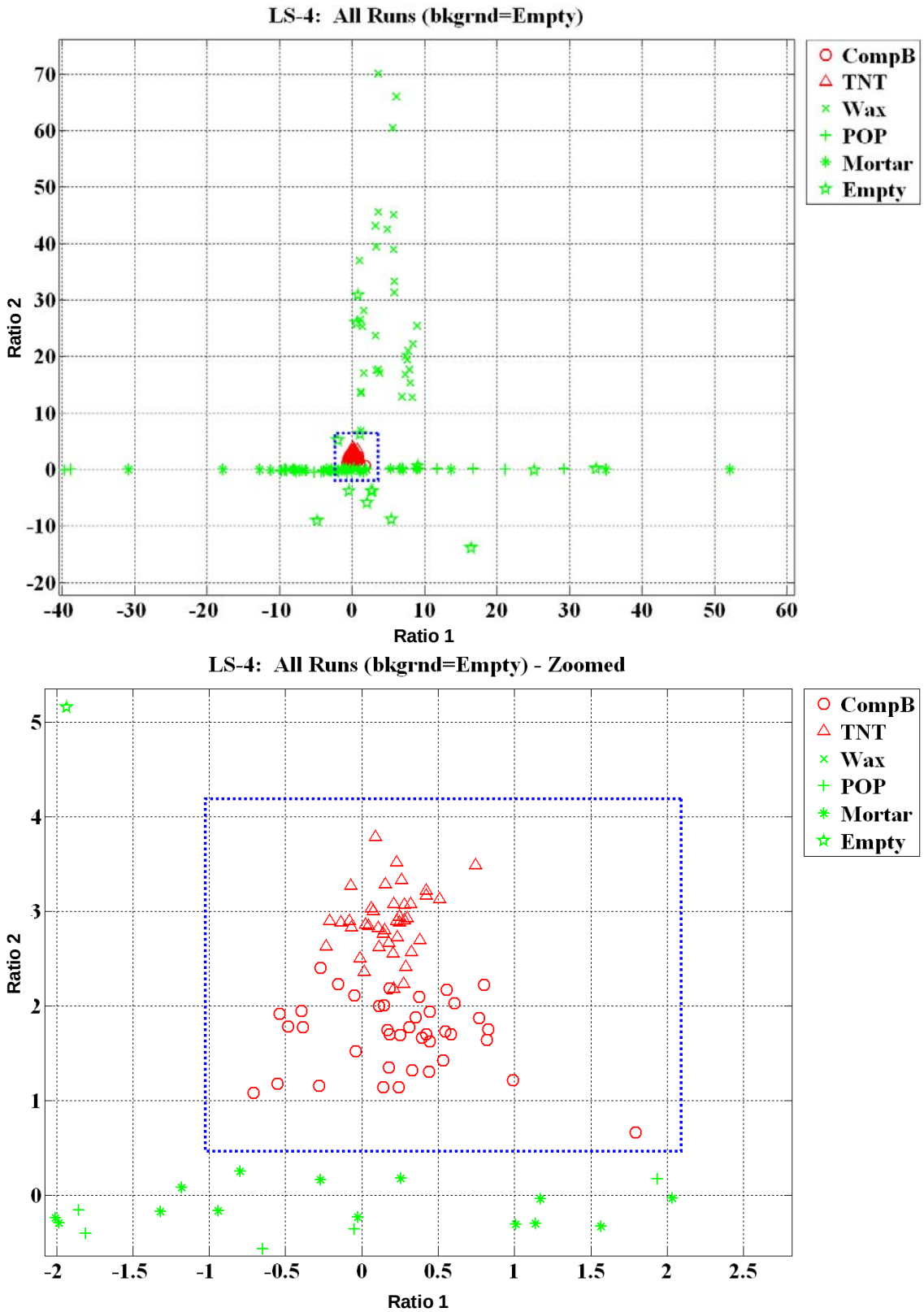

Figure 2.6-6. Plots of Ratios 2 versus 1 for the LS-4 configuration and with an empty shell in the background. The bottom plot is zoomed in over the blue box in the top plot.

LS Spectrum Analysis Conclusions

- Plots of elemental ratios show excellent discrimination between inert and explosive simulants.
- Distribution of inert and explosives simulants is tighter using an empty shell in the background than using no shell.
- Both BGO and $LaBr_3$ give very good results.
- Based on the excellent separation of inert and explosives simulants, Pdet = 100% and Pfa = 0% appear very likely.

GLRT Applied to LS

The LS results for the BGO and $LaBr_3$ detectors were provided to Duke University for applying GLRT as a decision maker and producing ROC curves. The detectors were analyzed individually with forced choice of explosives or non-explosives. The "Don't Know" decision was not considered in this analysis. An average of 100 ROCs was generated, each using 75% of the data for training and the remaining 25% of the data for testing. Figures 2.6-7 to 2.6-9 display the ROC curves for the elemental intensities and ratios for BGO and $LaBr_3$.

The results are very promising from the ROC curves, even without allowing a "Don't Know" declaration. It is possible to achieve 100% detection at less than 10% false alarm, and consistently achieve 100% detection at less than 20% false alarm. Allowing "Don't Know" declarations will likely reduce the 100% detection false alarms even further.

In general, the particular LS estimation method employed impacts performance. However, the affect is not always consistent and would require further investigation. The combination of elemental counts and ratios perform better than using only the counts or only the ratios with GLRT. The GLRT results are better with BGO data, and the energy detector is better with $LaBr_3$ data. There are inconsistencies between results with empty shell versus no shell also requiring further investigation.

Feature Set:
[C H N O Si]

BGO

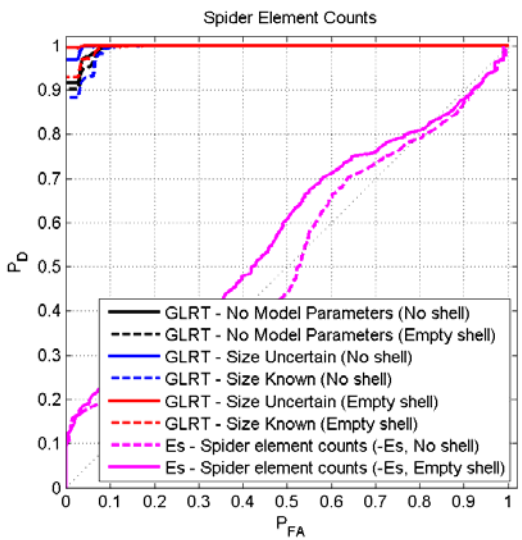

$LaBr_3$

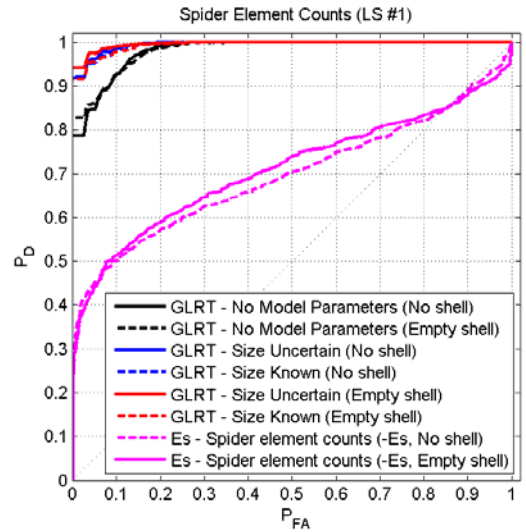

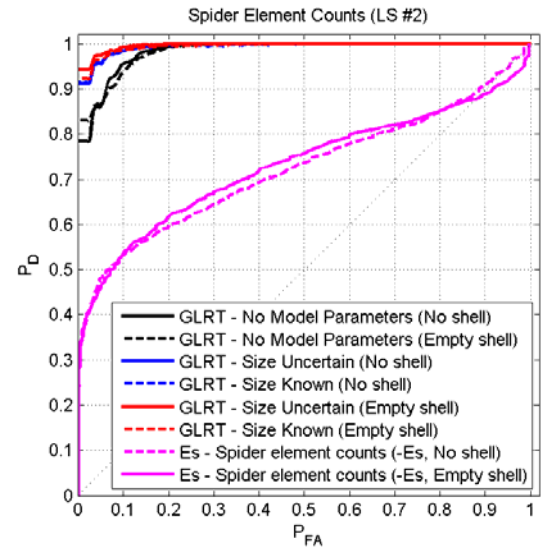

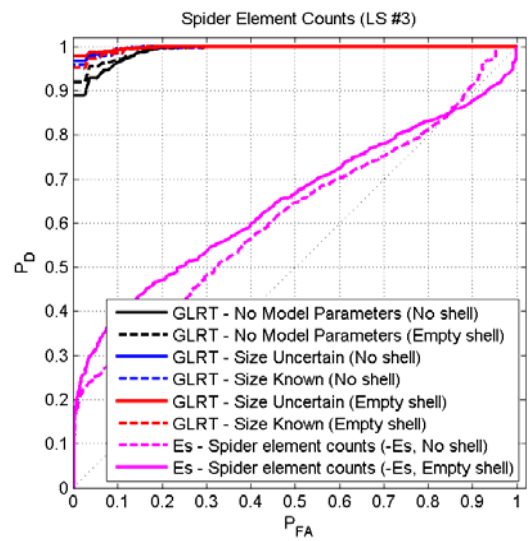

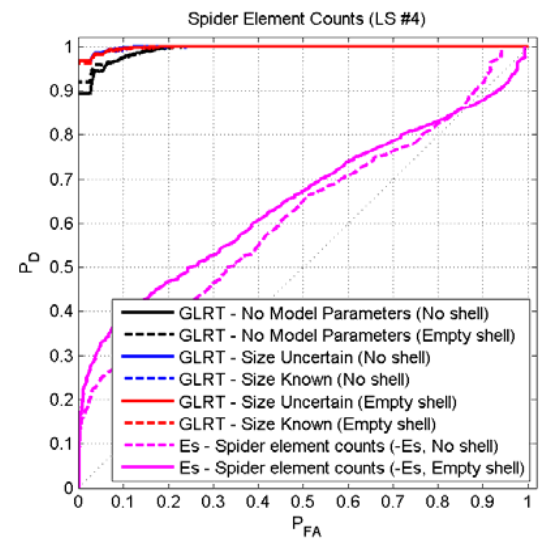

Figure 2.6-7. ROC curves generated using C, H, N, O and Si elemental intensities from the LS results for the BGO and $LaBr_3$ detectors.

Feature Set:
[C/O H/C]

BGO

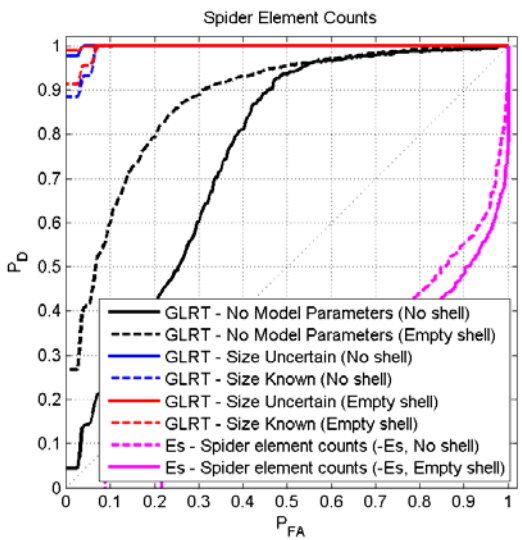

$LaBr_3$

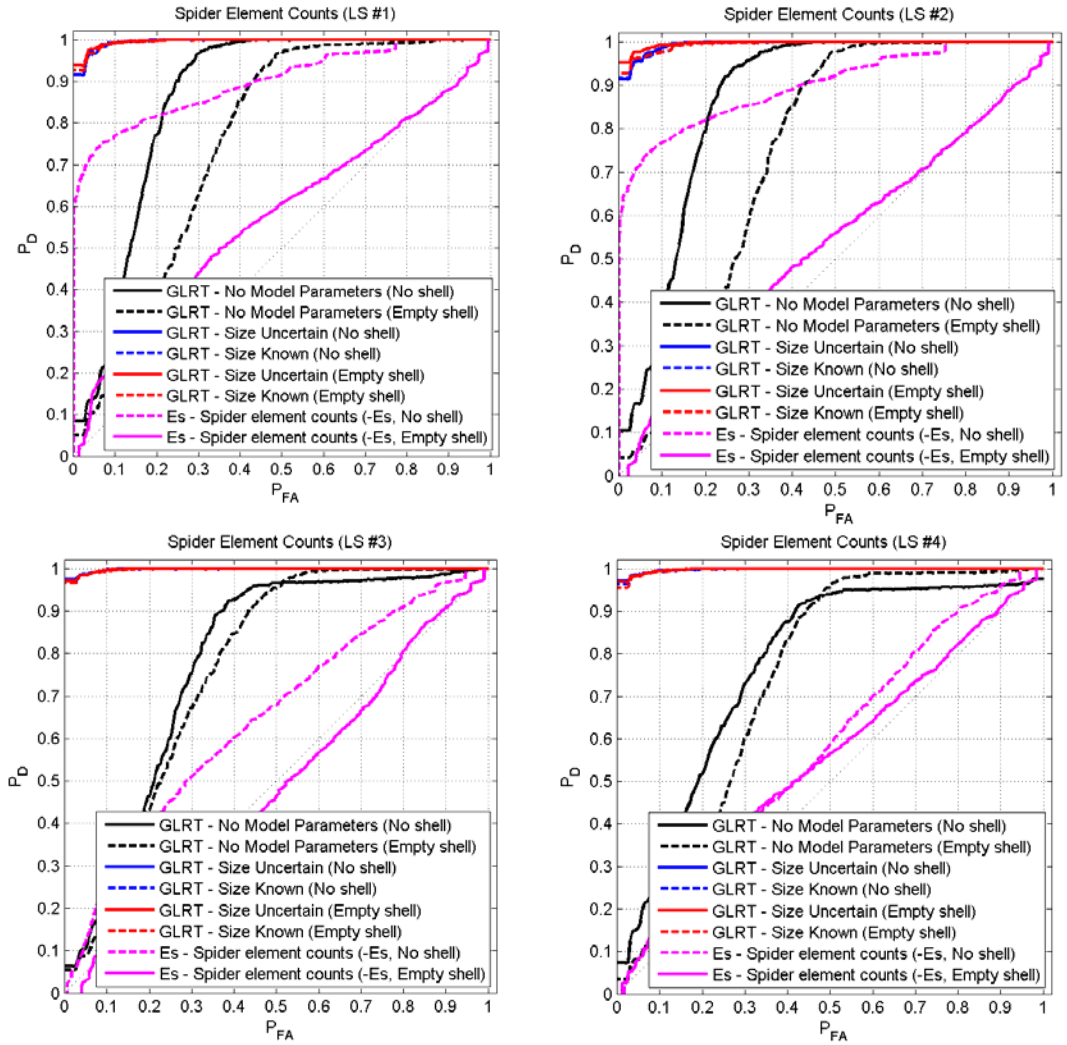

Figure 2.6-8. ROC curves generated using C/O and H/C elemental intensity ratios from the LS results for the BGO and $LaBr_3$ detectors.

Feature Set:
[C H N O Si C/O H/C]

BGO

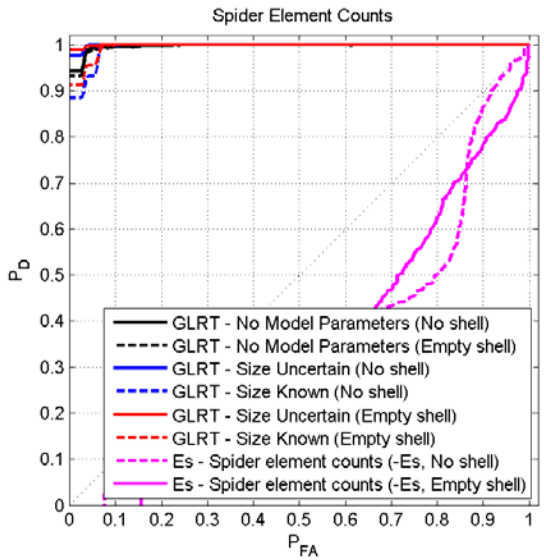

$LaBr_3$

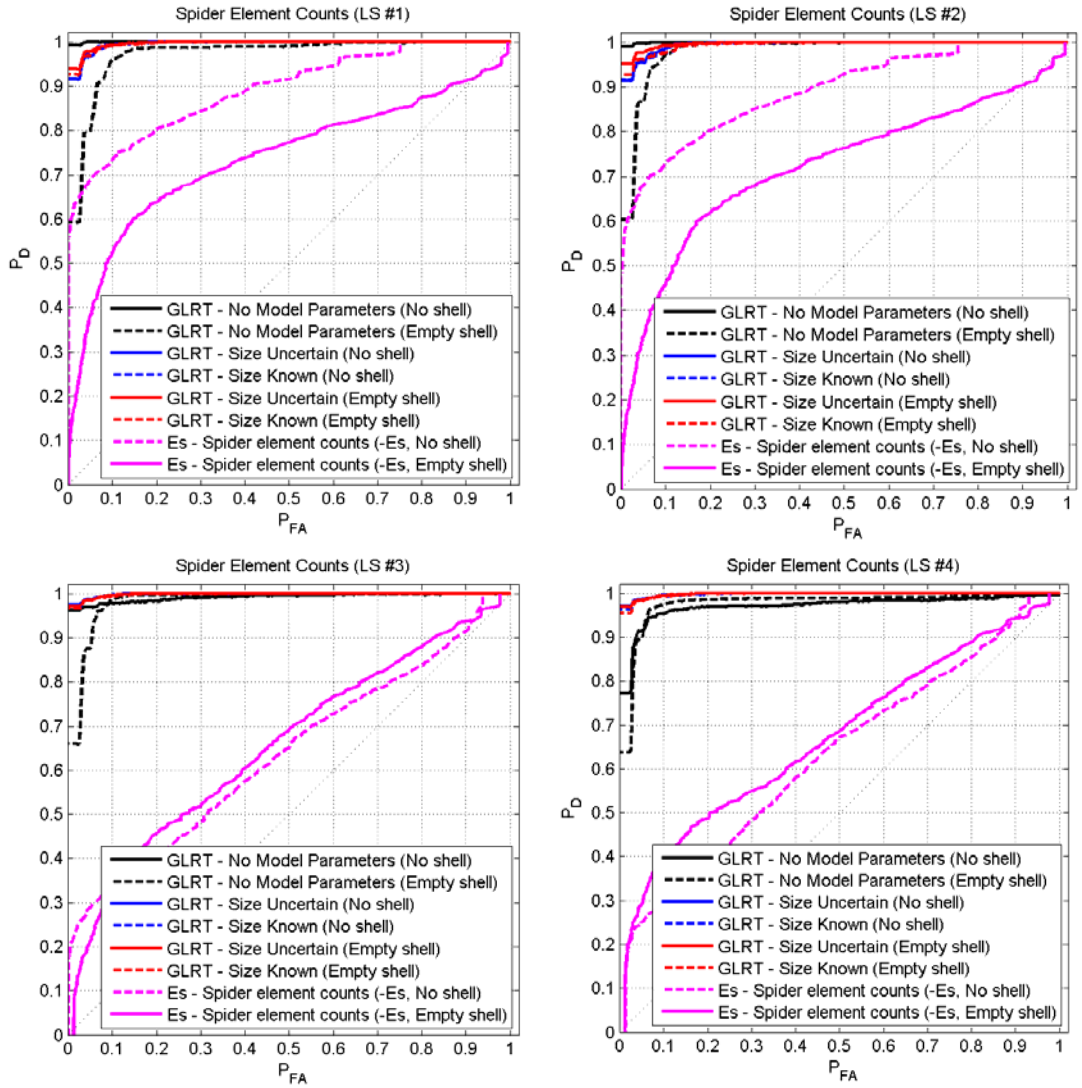

Figure 2.6-9. ROC curves generated using elemental intensities and ratios from the LS results for the BGO and LaBr3 detectors.

PCA Analysis and GLRT

In the PCA analysis of the spectra, the first three coefficients were used to generate ROC curves using a GLRT. Most of the data were well described by these first three components, and the results may be improved using more than three components, though the results were already very good. As with the LS results, an average of 100 ROCs were generated, each using 75% of the data for training and the remaining 25% of the data for testing. Figures 2.6-10 shows the ROC curves for the BGO and $LaBr_3$ detectors, Figure 2.6-11 shows the probability of correctly identifying a particular fill, and Figure 2.6-12 shows the probability of correctly identifying the class (explosive or inert) of a fill.

The results of the PCA/GLRT analysis are very promising even without allowing a "Don't Know" declaration. The results indicate that it is possible to achieve 100% detection at less than 10% false alarm. The performance consistently achieves 100% detection at less than 20% false alarm. Allowing a "Don't Know" declaration will likely reduce the 100% detection false alarms.

Other conclusions observed are that incorporating size uncertainty and utilizing both spectra improves performance. The results are consistent with performance predictions utilizing feature separability with the simulated data as described in a previous section.

Conclusions on BGO versus $LaBr_3$

Based upon the LS/GLRT and PCA/GLRT analysis, BGO consistently outperforms $LaBr_3$ for the explosives detection. However, neither detector consistently performed better for fill identification.

The results to date with fusion across spectra from a single detector demonstrate improved performance. Duke's suggestions were to investigate fusion across detectors and to determine the best feature set. The best result could be a combination of element counts, element count ratios, and PC coefficients from the four available spectra. Duke also suggested utilizing feature separability to predict the best features and to investigate the trade-off between spectral precision and uncertainty (from a signal processing perspective). $LaBr_3$ provides more precise peaks, but at the expense of greater location uncertainty.

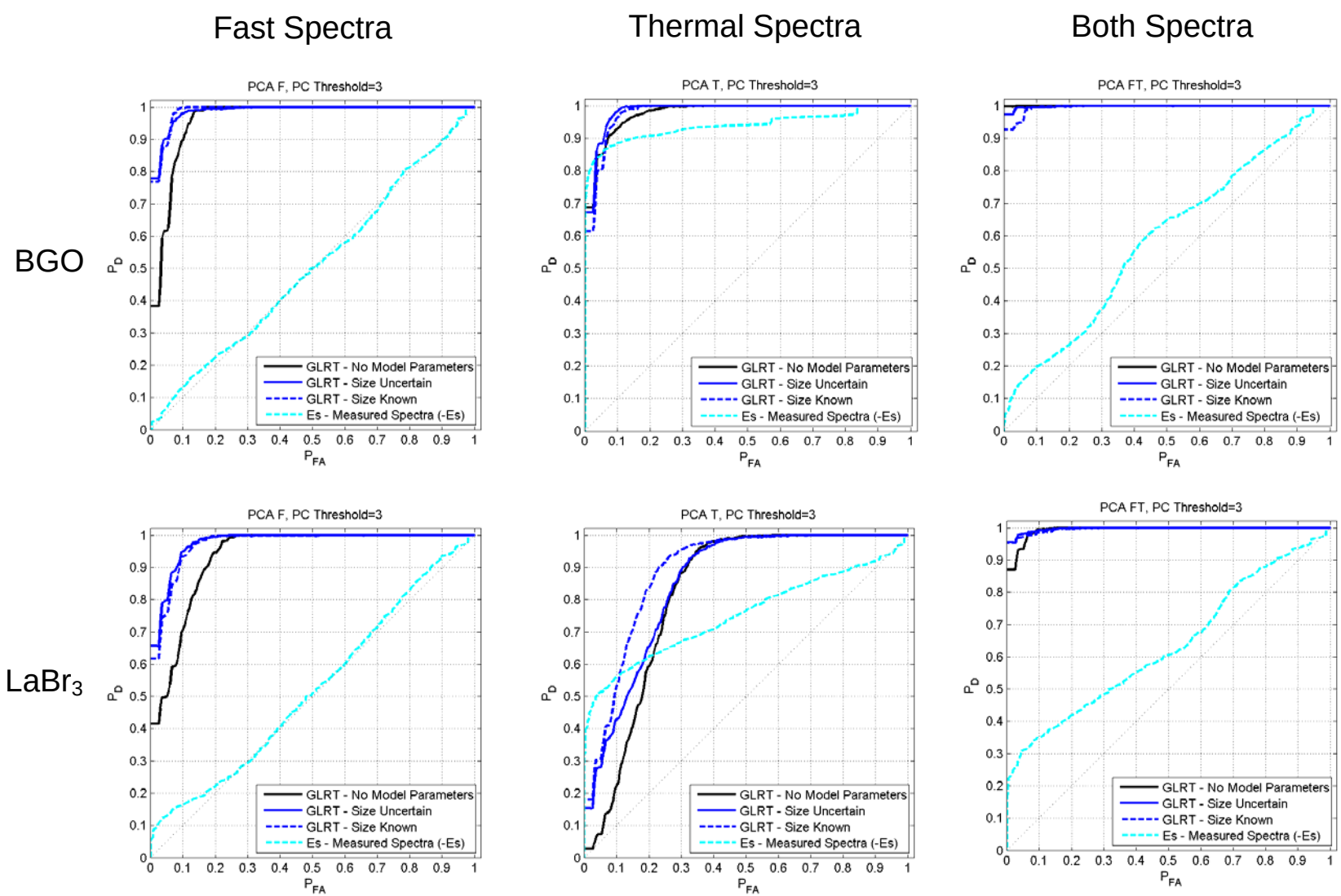

Figure 2.6-10. ROC curves for the PCA and GLRT analysis.

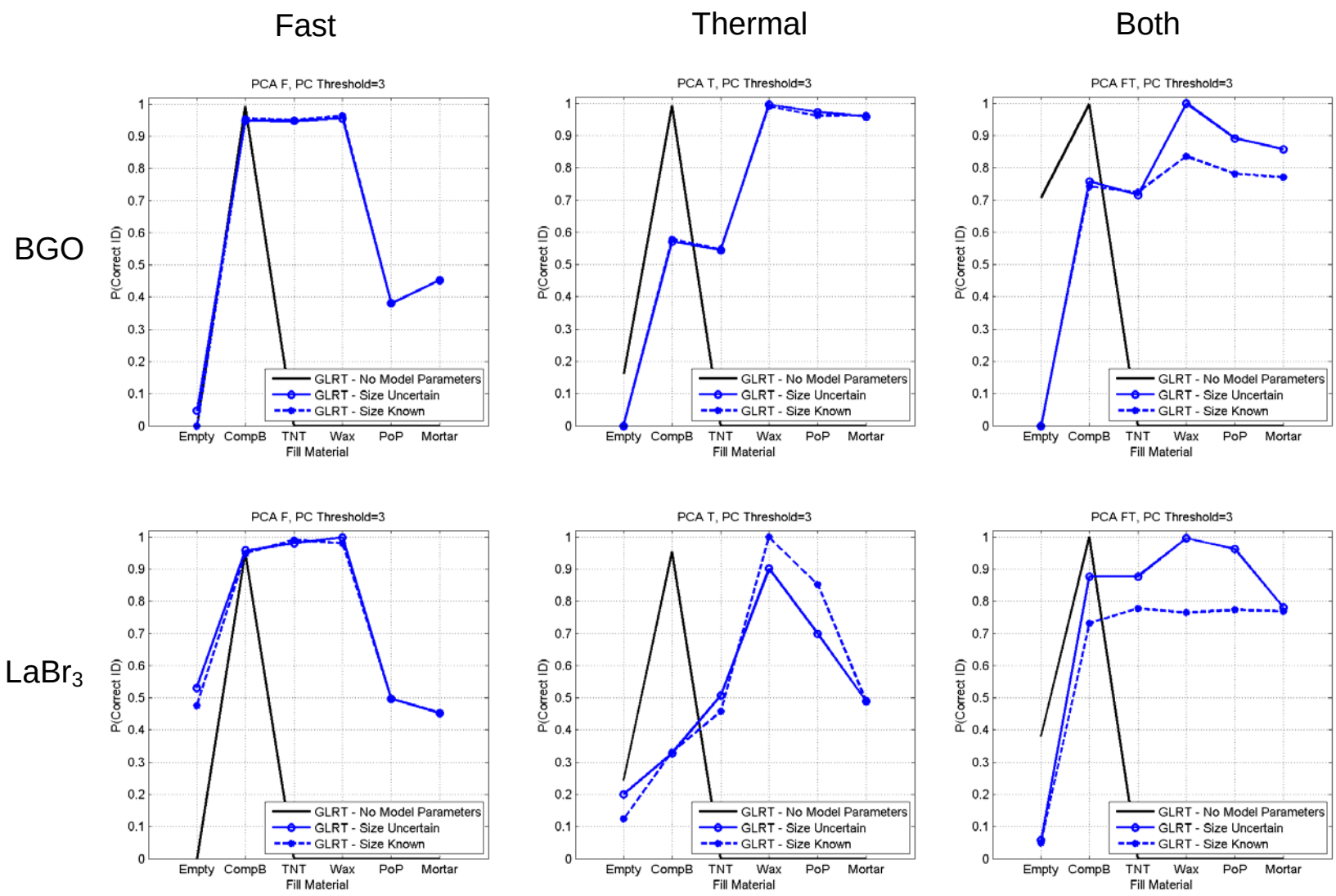

Figure 2.6-11. Probability that a fill is correctly identified.

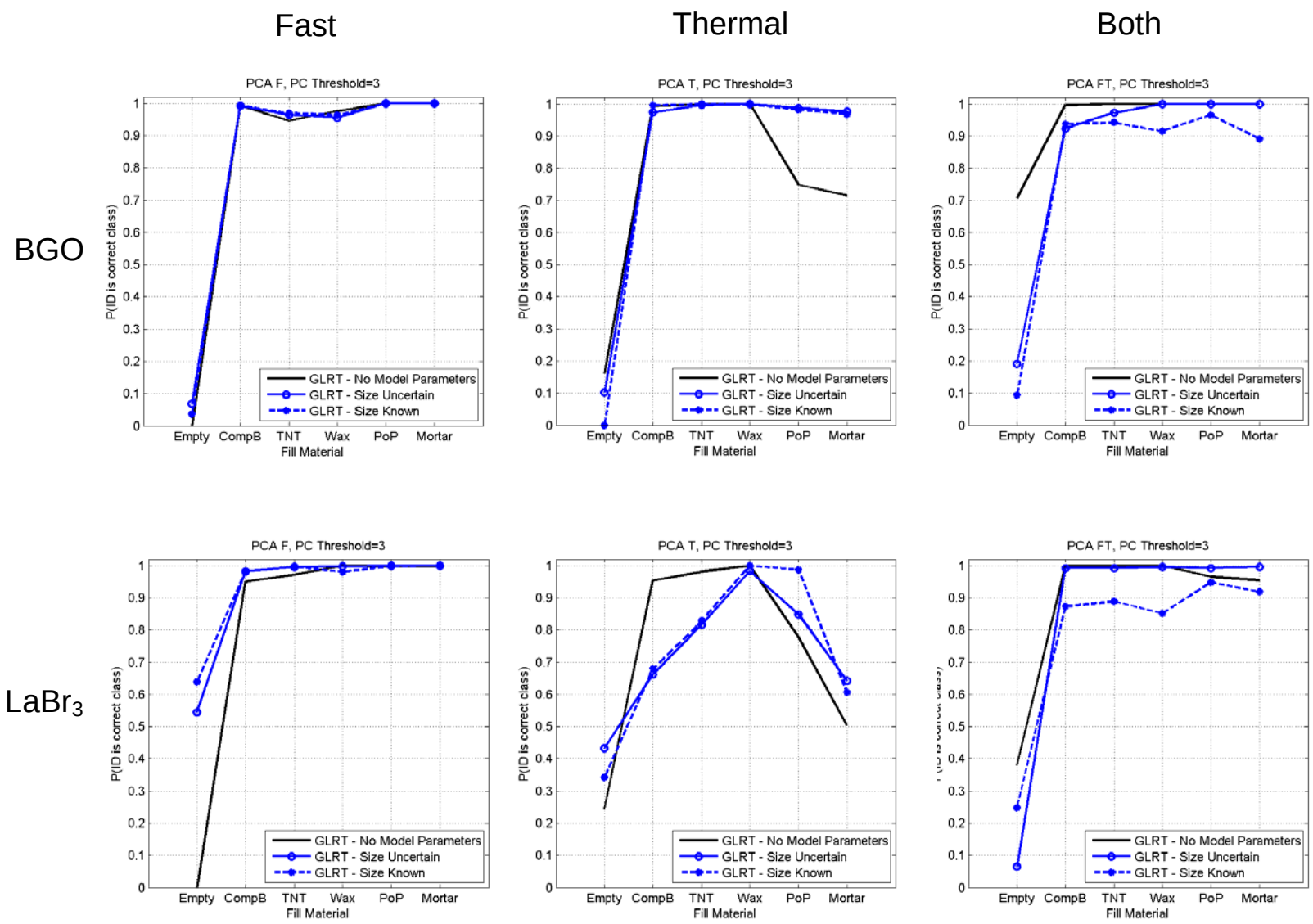

Figure 2.6-12. Probability that the fill class is correctly identified.

Overall Conclusions and System Design Recommendations

The experiments revealed very good performance discrimination between inert- and explosives-filled test slugs with Pdet=100% and Pfa=5%. The detection capability of BGO was, in general, greater than that for the $LaBr_3$ detector. Though $LaBr_3$ had three times the energy resolution of BGO, the lower stopping power played a significant role in performance (signal-to-noise).

2.7 Disposal Cost Examples and Payback Estimates

Disposal costs for UXO vary widely, dependent upon United States Environmental Protection Agency (EPA) and state regulatory environmental concerns (such as those experienced at Massachusetts Military Reserve), the type of site (e.g., military range or formerly used defense sites (FUDS), and location (i.e., isolated and/or uninhabited site versus a residential area such as Brooksville). For instance, at some sites, UXO deemed acceptable to move can be consolidated for disposal by detonation and a temporary on-site explosive storage site can be established for donor explosives. On other sites, such as Brooksville, disposal costs are considerably higher (labor, equipment, cost for donor explosives, requirement for on-time daily delivery of donor explosives versus on-site storage of donor explosives, etc.) due to additional measures that must be taken to protect the public and property. Average disposal-related costs experienced at MMR and Brooksville Turret Gunnery Range (TGR) are identified below.

Average Disposal Cost on MMR Total Environmental Restoration Contract (TERC)

The significant requirements in place at MMR for conduct of disposal of UXO by detonation increase directly related costs considerably to dispose of items determined unacceptable to move. As identified in the SAIC team briefing conducted for ESTCP on September 13, 2004, the average cost to conduct a BIP of one UXO item is approximately $650.

All UXO acceptable to move at MMR, including live items and items that are suspected to be live, are stockpiled for disposal by another contractor in the contained detonation chamber (CDC). The CDC is brought to MMR to dispose of these UXO items for a 30-day period approximately once every seven to eight months to destroy stockpiled UXO at a cost of approximately $250,000 per 30-day period. A daily rate of $5,000 per day is assessed for each day over 30 days. The number of items that can be destroyed in a 30-day period varies widely depending on the types of items to be disposed. For example, if mainly small items are being disposed (i.e., detonators out of fuzes, pieces of 40mm rounds), approximately 7,000 items can be disposed of in a 30-day period. If 60mm and 81mm mortars are being disposed, approximately 500 mortars can be disposed of in a 30-day period (20 to 25 rounds per day times 22 work days), which equates to approximately $500 per item.

During 2005-2006, ECC conducted tests using other technologies and procedures. ECC was able to positively certify that 805 out of 830 stockpiled mortars (60mm and 81mm) were free of explosives and, following proper procedures, could be disposed of as munitions scrap. The cost to demilitarize (i.e., cut) and dispose of these items as scrap is a minor cost as compared to disposal by detonation utilizing BIP procedures or in the CDC, which results in a significant cost savings.

Average Disposal Cost on Brooksville TGR

ECC's average cost for disposal by detonation of UXO at Brooksville TGR during 2005-2006 was $794 per shot, not including the cost to plan for and conduct evacuation of residents. The high cost of disposal on this site was due to its location. The project was conducted in a large, densely populated housing area that required a significant amount of additional safety measures, labor, equipment and daily "on time" delivery of explosives coming from Tampa, Fla., (approximately 60 miles from Brooksville). UXO that were determined to be live rounds and those that could not be positively identified as free of explosives were disposed of by detonation. Upon detonation, a large percentage of the detonated UXO items were determined to be free of explosives. ECC performed 284 disposal shots on this site, of which 19.7% were determined to be live HE rounds and 80.3% were determined to be UXO that did not, in fact, contain explosives.

Anticipated Payback Using Advanced PELAN

To estimate the savings in using PELAN over a 10-year period, we first estimated the cost assessment for each PELAN system.

- Operational: Two-man hour per inspection or approximately $100 per inspection
- Capital acquisition cost: $250,000
- Annual maintenance, training and regulatory cost : $10,000
- Lifetime system maintenance costs (10 years): $100,000
- Assume one NG tube replacement over life of system
- Total capital and maintenance costs: $350,000

For the estimated payback for use at MMR and similar sites, we assumed the following based on ECC's experience.

- Cost savings per inspection: Approximately $500 per inspection
- Excludes savings associated with treating soil contaminated by explosives
- Number of inspections on inert shells per day: 15 (out of 30 total inspections)
- Cost savings over 10 years (39,000 shots): $19.5 million for each system

So the approximate net savings over 10 years is about $19 million for each system.

2.8 Final Conceptual Design

Based on operational requirements, results from MCNP modeling and laboratory experimentation, a final conceptual design for the UXO discrimination system was developed. The system was designed to accommodate UXO excavated and stockpiled onsite with emphasis on 100% detection and discrimination between inert and explosive fills with identification in one minute or less. The system focused two gamma-ray detectors on the center-of-mass of the UXO under inspection, similar to the laboratory system. A neutron generator located at the top of the

system irradiated down on the ordnance. Automated software controlled the data acquisition and provided a result of inert, explosives, or unknown.

Although the laboratory testing showed that BGO detectors performed better than $LaBr_3$, the system was designed to accommodate either detector.

The overall weight of the system was estimated at 1,800 pounds and ultimately would be transported in a small trailer.

The operator interface for the system, located on the control laptop, is shown in Figure 2.8-1. The interface software is based off of the PELAN system. Re-using a large portion of the PELAN software helped to minimize the overall cost for the prototype system. The software controls the neutron generator and the data acquisition electronics, displaying the final result as inert, explosives, or unknown. The final analysis could be selectable between two possible algorithms; LS/GLRT or PCA/GLRT.

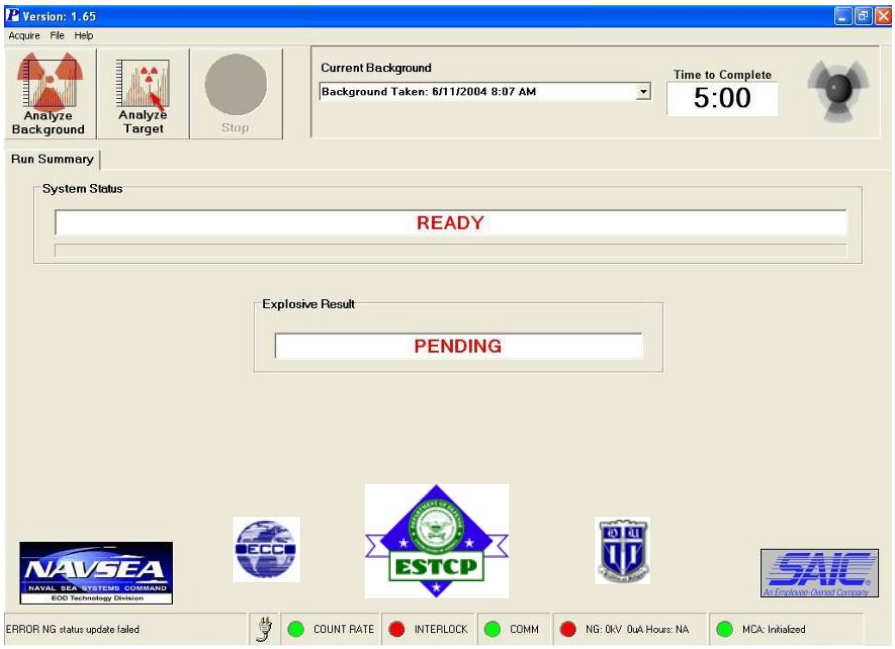

Figure 2.8-1. Software User Interface

3. OVERALL CONCLUSIONS

A laboratory model of a stationary inspection system based on PELAN technology was built and tested in the laboratory. Targets (slugs) were constructed that represented a range of UXO in both size and fill capacity. The fills used in the testing were Comp B and TNT explosives simulants, mortar, plaster of Paris, wax and empty fills. Three types of detectors were tested: a 3-inch by 3-inch $LaBr_3$, 3-inch by 3-inch BGO, and 5-inch by 6-inch NaI. The 3-inch by 3-inch $LaBr_3$ detector was one of the first large volume La-halide detectors made commercially by Saint-Gobain and had an energy resolution at 662 keV of 3%, at least three times better than that

for the BGO detector. Though $LaBr_3$ had excellent resolution, the higher stopping power (detection efficiency) of BGO led to its better performance for UXO discrimination.

Based upon the modeling and test results, we make the following key conclusions:

- Discrimination between inert and explosives-filled test slugs using one detector is excellent (Pdet=100%/Pfa=5%).
  - Would improve when utilizing two or more detectors (data fusion)
- Utilize two 3-inch by 3-inch BGO detectors.
  - Shorter examination times are realized with multiple detectors (approximately one minute per inspection)
  - Additional analysis using a combination of BGO and LaBr3 is warranted because they could provide complementary information
  - More studies are recommended to examine the benefits of the much faster decay times of $LaBr_3$ for reducing pileup effects and shortening inspection times

- Cost savings are estimated to be about $19 million over 10 years for eliminating BIP for each inert or empty shell.

4. References

[1] A. Webb. *Statistical Pattern Recognition*. John Wiley & Sons, 2nd Edition, 2002
[2] R.O. Duda, P.E. Hart, and D.G. Stork. *Pattern Classification*. John Wiley & Sons, Inc., 2001.

5. Points of Contact

Point of Contact Name	Organization Name and Address	Role in Project
Robert Sullivan	10740 Thornmint Road San Diego, CA 92127 Ph: 858-826-6019 Fax: 858-826-7618 Email: Robert.a.sullivan@saic.com	Project Lead
Daniel Holslin	10740 Thornmint Road San Diego, CA 92127 Ph: 858-826-9715 Fax: 858-826-7618 Email: Daniel.t.holslin@saic.com	Principal Investigator
Kurt Hacker	NAVEODTECHDIV Code 5011F 2008 Stump Neck Road Indian Head, MD 20640 Ph: 301-744-6850	Contracting Officer's Technical Representative (COTR)
Stacy Tantum	Duke University 3453 FCIEMAS Durham, NC 27708 Ph: 919-660-5239 Fax: 919-660-5293 Email: stacy.tantum@duke.edu	Algorithm Development and Data Analysis
Leslie Collins	Duke University 3461 Fitzpatrick Center Phone: 660-5260, 660-5212 Fax: 660-5293 Email: lcollins@ee.duke.edu	Algorithm Development and Data Analysis
Doug Lamothe	Environmental Chemical Corporation 4825 University Square, Suite 3 Huntsville, AL 35816 Ph: 256-217-1565 Fax: 256-217-1566 Email: dlamothe@ecc.net	Establishing user requirements/CONOPS*, providing ordnance specifications, and guidance on system design
Glenn Earhart	Environmental Chemical Corporation 4835 University Square, Suite 10 Huntsville, AL 35816 Tel: 256-217-1565, x102 Fax: 256-217-1566 Email: gearhart@ecc.net	Establishing user requirements/CONOPS, providing ordnance specifications, and guidance on system design

CONOPS = concept of operations